

GEOCHEMICAL AND ISOTOPIC EVOLUTION OF THE ANORTHOSITIC PLUTONS OF THE LARAMIE ANORTHOSITE COMPLEX: EXPLANATIONS FOR VARIATIONS IN SILICA ACTIVITY AND OXYGEN FUGACITY OF MASSIF ANORTHOSITES

CAROL D. FROST[§] AND B. RONALD FROST

Department of Geology and Geophysics, University of Wyoming, Laramie, Wyoming 82071, USA

DONALD H. LINDSLEY

Department of Geosciences and Mineral Physics Institute, Stony Brook University, Stony Brook, New York 11794-2100, USA

KEVIN R. CHAMBERLAIN AND SUSAN M. SWAPP

Department of Geology and Geophysics, University of Wyoming, Laramie, Wyoming 82071, USA

JAMES S. SCOATES

Department of Earth and Ocean Sciences, University of British Columbia, Vancouver, British Columbia V6T 1Z4, Canada

ABSTRACT

The Laramie anorthosite complex includes three anorthositic plutons: the Poe Mountain, Chugwater, and Snow Creek intrusions. The Poe Mountain and Chugwater bodies exhibit mappable magmatic stratigraphy that records fractionation processes in a magma chamber at or near the present level of exposure followed by doming and expulsion of residual liquid. The Snow Creek pluton is more poorly exposed, although layering is locally observed, and there is geochemical evidence for removal of interstitial liquid in the eastern portion of the body. The three plutons were emplaced in close succession. The U–Pb zircon and baddeleyite geochronology of anorthosite from the Chugwater and Snow Creek plutons, and a monzodiorite dike, indicates that the Chugwater is the oldest of the bodies, with a weighted average ²⁰⁷Pb/²⁰⁶Pb age of five samples of 1435.5 ± 0.3 Ma. The Snow Creek anorthosite intrudes the previously dated 1434 Ma Poe Mountain anorthosite and is, in turn, cut by the 1432.8 ± 2.4 Ma monzodiorite dike. The LAC and associated granites of the Sherman batholith suite were emplaced over a period no greater than 12 million years, and possibly in as little as three million years. Despite their similar ages, each of the LAC anorthosite plutons displays a distinctive assemblage of minerals. The Poe Mountain anorthosite is characterized by olivine, augite, low Ca-pyroxene, ilmenite and magnetite, and plagioclase in the range An_{43–53}. The Chugwater anorthosite generally contains no olivine but is composed of augite, low Ca-pyroxene, ilmenite and magnetite, and iridescent plagioclase in the range An_{50–56}. The Snow Creek anorthosite is characterized by a lack of olivine and magnetite and the presence of iridescent plagioclase of composition An₄₇ to An₅₆; it is commonly quartz-bearing. These assemblages record a range of silica activities and oxygen fugacities. Higher activities of silica and fugacities of oxygen are correlated with greater amounts of crustal assimilation, as indicated by Nd and Sr isotopic compositions and the presence of inherited components in zircon. We demonstrate that crustal assimilation can produce a range of mineral assemblages and Sr–Nd isotopic compositions in LAC anorthosites crystallized from common mantle-derived parental magmas, and that assimilation of crust is likely an important control on the compositional variations documented in other Proterozoic massif anorthosites.

Keywords: anorthosite, silica activity, oxygen fugacity, geochronology, Nd and Sr isotopes, Laramie anorthosite complex, Wyoming.

SOMMAIRE

Le complexe anorthositique de Laramie contient trois plutons majeurs, Poe Mountain, Chugwater, et Snow Creek. Les massifs de Poe Mountain et de Chugwater font preuve d'une stratification ignée qui témoigne de processus de fractionnement dans une chambre magmatique près du niveau actuel d'affleurement, ceci suivi d'un soulèvement et d'une expulsion du liquide résiduel.

[§] E-mail address: frost@uwyo.edu

Le pluton de Snow Creek affleure moins bien, quoiqu'un litage soit observé localement, et il existe des signes géochimiques favorisant l'évacuation d'un liquide interstitiel dans la partie orientale du pluton. Les trois plutons ont été mis en place dans un court laps de temps. L'étude géochronologique U–Pb effectuée sur le zircon et la baddeleyite prélevés de l'anorthosite des plutons de Chugwater et de Snow Creek, ainsi que d'un filon de monzodiorite, montre le pluton de Chugwater serait le plus ancien de ces venues, avec une moyenne d'âges $^{207}\text{Pb}/^{206}\text{Pb}$ pondérée de 1435.5 ± 0.3 Ma (cinq échantillons). L'anorthosite de Snow Creek recoupe le massif de Poe Mountain, déjà daté (1434 Ma) et il est, à son tour, recoupé par le filon de monzodiorite (1432.8 ± 2.4 Ma). Le complexe anorthositique de Laramie et les granites associés du batholite de Sherman ont été mis en place au cours d'un intervalle de pas plus que 12 millions d'années, et peut-être même aussi peu que trois millions d'années. Malgré leurs âges semblables, chacun des plutons anorthositiques présente un assemblage distinctif de minéraux. L'anorthosite de Poe Mountain contient olivine, augite, pyroxène à faible teneur en Ca, ilménite et magnétite, et un plagioclase dans l'intervalle An_{43-53} . L'anorthosite de Chugwater ne contient pas d'olivine, en général, mais possède l'assemblage augite, pyroxène à faible teneur en Ca, ilménite et magnétite, un plagioclase iridescent de composition An_{50-56} . Dans l'anorthosite de Snow Creek, l'olivine et la magnétite sont absentes, et le plagioclase, de composition An_{47} to An_{56} , est iridescent, et le quartz est présent, en général. Ces assemblages témoignent d'un intervalle d'activités de silice et de fugacités d'oxygène. Les valeurs plus élevées de ces paramètres montrent une corrélation avec une assimilation accrue de la croûte, comme l'indiquent les compositions isotopiques du Nd et du Sr, ainsi que la présence de composantes héritées dans le zircon. Nous démontrons que l'assimilation de la croûte peut produire un éventail d'assemblages de minéraux et de compositions isotopiques Sr–Nd dans le complexe anorthositique de Laramie à partir du même magma parent dérivé du manteau, et qu'elle exercerait un contrôle important sur les variations en composition documentées dans d'autres massifs protérozoïques d'anorthosites.

(Traduit par la Rédaction)

Mots-clés: anorthosite, activité de silice, fugacité d'oxygène, géochronologie, isotopes de Nd et de Sr, complexe anorthositique de Laramie, Wyoming.

INTRODUCTION

Although all massif anorthosites are by definition dominated by plagioclase, they evince a wide range of compositional and mineralogical variability. Massif anorthosites may be subdivided on the basis of plagioclase composition into andesine and labradorite anorthosites (Anderson & Morin 1969). Massif anorthosites also differ in their silica activity and oxygen fugacity (Hébert *et al.* 2005, Morse 2006). Andesine anorthosites, such as Labrieville (Owens & Dymek 2001), are commonly quartz-saturated, contain exsolved ferrian ilmenite (commonly known as “hemo-ilmenite”, so named for the presence of exsolved lamellae of hematite in an ilmenite host), and typically lack magnetite. Labradorite anorthosites usually lack quartz, commonly contain olivine, and are characterized by coexisting ilmenite and magnetite. However, even within the labradorite anorthosites such as the Nain Plutonic Suite, there is a considerable range in silica activity and oxygen fugacity, from reduced and olivine-saturated to relatively oxidized and quartz-saturated (Xue & Morse 1993). The causes for these variations in intensive conditions remain uncertain. Owens & Dymek (2001) contended that they reflect differences in the primary magmas of anorthosites, whereas Xue & Morse (1993) argued that the range of compositions is related to crustal assimilation.

In this contribution, we describe three anorthositic plutons from the 1.44 Ga Laramie Anorthosite Complex (LAC) that are exposed in a relatively small area (~800 km²) in the Laramie Mountains of southeastern Wyoming, USA. We present geochronological, petro-

logical and geochemical results to document that these plutons were intruded over a short period of time, and that they record a similar a range of silica activity and oxygen fugacity as the much larger and longer-lived Nain Plutonic Suite, Labrador. Because the anorthositic plutons of the LAC were intruded close in space and time and under the same tectonic conditions, the variables that control the differences in oxidation state and silica activity can be reasonably well constrained. Moreover, because the LAC intrudes Archean and Proterozoic wallrocks that are considerably older than the anorthositic plutons, Nd and Pb isotopic compositions of the LAC are sensitive indicators of crustal contamination. Thus, the LAC affords an opportunity to evaluate the processes by which massif anorthosites obtain their varying compositions.

ANORTHOSITIC PLUTONS OF THE LARAMIE ANORTHOSITE COMPLEX

The Laramie Anorthosite Complex (LAC) is exposed in the Laramie Mountains of southeastern Wyoming, a Laramide uplift that has been thrust over Phanerozoic rocks along its eastern margin (Fig. 1). The western contact of the complex is overlain by Phanerozoic sedimentary rocks. Only the northern and southern contacts of the complex are well exposed. The LAC intruded the *ca.* 1.75 Ga suture between the Archean Wyoming province and Proterozoic crust. To the north lies the Archean Wyoming province that is dominated by Late Archean granitic gneisses. To the south lie Proterozoic rocks that were formed at 1.76 Ga or earlier. The Archean–Proterozoic boundary dips

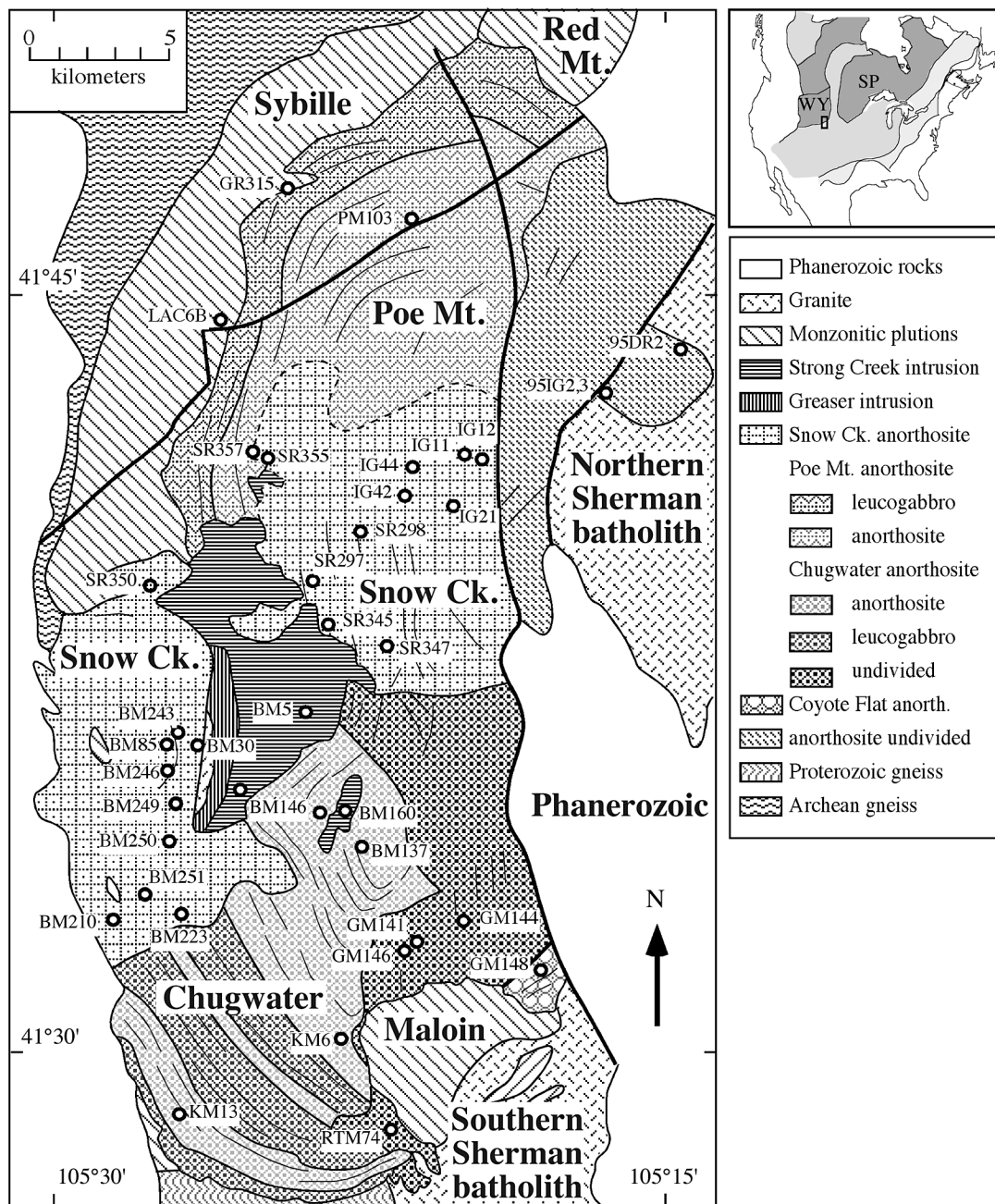


FIG. 1. Simplified geological map of the Laramie anorthosite complex, southeastern Wyoming, showing the locations of the Poe Mountain, Snow Creek, and Chugwater anorthosite plutons, and sample locations for geochemical, isotopic and mineral chemistry results presented in this study. The inset map shows the location of the LAC on the southeastern margin of the Archean Wyoming province. The Cheyenne belt, which marks the trace of the Archean-Proterozoic boundary, is constrained to lie north of the Proterozoic gneisses intruded by the Chugwater anorthosite and south of the southernmost exposures of Archean rocks intruded by the western Snow Creek anorthosite. The suture dips to the southeast at approximately 55° (Allmendinger *et al.* 1982); therefore, the Poe Mountain anorthosite ascended exclusively through Archean-age crust, and the southern Chugwater anorthosite traversed the greatest thickness of Proterozoic-age crust.

approximately 34° to the south (Allmendinger *et al.* 1982, Chamberlain 1998).

The LAC consists of three anorthosite plutons: Poe Mountain (Scoates 1994, 2000, Scoates & Frost 1996), Chugwater (Lindsley *et al.* 2010), and Snow Creek anorthosites, two mafic intrusions, the Strong Creek and Greaser intrusions (Mitchell 1993, Mitchell *et al.* 1995, 1996), and three monzonitic plutons, Sybille (Fuhrman *et al.* 1988, Scoates *et al.* 1996), Maloin (Kolker & Lindsley 1989, Kolker *et al.* 1990, 1991), and Red Mountain (Anderson *et al.* 2003) plutons, along with numerous small plutons and dikes of high-Al gabbro, leucotroctolite, ferrodiorite, monzodiorite, and granite. The LAC is spatially and temporally associated with the 1438–1431 Ma ferroan, alkalic–calcic Sherman batholith, which is exposed along the northeastern and southern margins of the LAC (Geist *et al.* 1989, Frost *et al.* 1999, 2001, 2002, Edwards & Frost 2000).

The anorthositic plutons

The anorthositic plutons are the oldest intrusive rocks in the LAC. They form the core of the complex and are rimmed by younger intrusions (Fig. 1). The Poe Mountain anorthosite, which is the northernmost anorthositic pluton, is a distinctly layered intrusion that grades from anorthosite in the lower stratigraphic levels to leucogabbro in the higher levels (Scoates 1994, 2000). Layering in the Poe Mountain anorthosite forms a domal pattern with dips becoming progressively shallower toward lower stratigraphic levels. Most of the eastern portion of the dome has been disrupted by Laramide faults, so that only the western and northern margins are preserved. The Poe Mountain anorthosite is characterized by olivine, augite, low-Ca pyroxene, ilmenite and magnetite, and plagioclase (An_{43–53}). The Poe Mountain anorthosite contains numerous blocks of leucogabbro that deform the plagioclase lamination beneath them; these are interpreted as representing blocks that dropped through an open magma chamber onto the floor of the intrusion. The source of the blocks may be preserved as large xenoliths of leucogabbro that occur within the northern portion of the Sybille intrusion. Locally within these xenoliths, the leucogabbro is chilled against the Archean country rock. Three samples of Poe Mountain anorthosite give U–Pb zircon or baddeleyite ages that are identical within error: 1434.4 ± 0.6, 1434.5 ± 0.6, and 1434.1 ± 0.7 Ma (Scoates & Chamberlain 1995).

The southern anorthositic pluton of the LAC is the Chugwater anorthosite (Lindsley *et al.* 2010). The Chugwater anorthosite consists of broad layers of anorthosite and gabbroic anorthosite. Unlike the Poe Mountain anorthosite that formed by *in situ* fractionation in a mid-crustal-level magma chamber (Scoates *et al.* 2010), the Chugwater anorthosite was emplaced as a series of crystal-rich magmas followed by doming, probably in response to gravitational instability of a plagioclase-rich

crystal-rich mush (Lindsley *et al.* 2010). Like the dome of the Poe Mountain anorthosite, the eastern limb of the dome has been greatly affected by later deformation. Some of this deformation occurred at a high temperature and may have been related to the emplacement of the Maloin Ranch pluton, whereas some of it is clearly associated with brittle deformation during the Laramide orogeny. The Chugwater anorthosite contains augite, low-Ca pyroxene, ilmenite and magnetite, and plagioclase in the range An_{50–56} (Lindsley *et al.* 2010). Anorthosite in the Chugwater pluton generally contains no olivine and is locally quartz-bearing. Olivine is present where the anorthosite has been intruded by and mixed with leucotroctolite. Scoates & Chamberlain (1995) reported one U–Pb baddeleyite date, 1435.5 ± 0.5 Ma, from the northern part of the Chugwater anorthosite, which overlaps within error the dates obtained for the Poe Mountain anorthosite.

The relative ages of the Poe Mountain and Chugwater anorthosites cannot be determined from field relations because the Snow Creek anorthosite lies between them (Fig. 1). The Snow Creek anorthosite had received relatively little attention prior to this study, in part because outcrop is limited and contacts are poorly exposed. The Snow Creek anorthosite is intruded by the troctolitic Strong Creek and ferrodioritic Greaser mafic intrusions (Mitchell 1993), which divide the anorthosite into western and eastern portions. The pluton is named for exposures in the Snow Creek area on the central–western portion of the LAC. In this area, the Snow Creek anorthosite is weakly layered, with the layering having a nearly flat orientation. In the eastern portion of the Snow Creek anorthosite, the layering is steeper and better developed, but this area is more highly deformed than the western Snow Creek region. The Snow Creek anorthosite is characterized by a lack of magnetite and the presence of iridescent plagioclase. It is commonly quartz-bearing, particularly the western portion. Both the southern and northern intrusive contacts of the western body are sharp and are delineated by changes in fabric orientation. In contrast, the limits of the eastern body are very difficult to delineate. We established these limits by noting the locations of samples that lack magnetite in thin section.

There is a sizable area of anorthosite in the northern portion of the complex that is bounded on all sides by Laramide faults. Because the rocks are extensively altered, we are unable to determine to which pluton these rocks belong. Consequently, we have mapped it as “anorthosite undivided”.

GEOCHRONOLOGY OF THE CHUGWATER AND SNOW CREEK ANORTHOSITES

Only one date has been published from the Chugwater pluton, and none from the Snow Creek pluton. Accordingly, we present in this study U–Pb isotopic compositions of four baddeleyite and 18 zircon fractions

(Table 1) from six samples: four from the Chugwater anorthosite, one sample from the Snow Creek anorthosite, and one sample from a late monzodiorite dike that cross-cuts the Snow Creek anorthosite. Between nine and 20 grains of baddeleyite and between one and 17 grains of zircon were dissolved for each analysis.

Zircon in most samples is anhedral and colorless. Scoates & Chamberlain (1995) interpreted anhedral zircon in the Laramie anorthosite complex as a late-

crystallizing phase interstitial to cumulus plagioclase. Two samples contain predominantly euhedral zircon: GM148 from the Coyote Flat area of the Chugwater anorthosite, and BM5 from the monzodiorite dike. Baddeleyite was analyzed from two samples. The analyzed grains are brown and translucent, and many grains display well-developed polysynthetic twinning.

Concentrations of U and Pb are extremely low, ranging from 79 to 588 ppm U and 19 to 158 ppm Pb.

TABLE 1. U-Pb ZIRCON AND BADDELEYITE DATA, LARAMIE ANORTHOSITE COMPLEX, WYOMING

| Mineral fraction | Weight | U | Pb | Pb _c | ²⁰⁶ Pb/ ²⁰⁸ Pb ^a | ²⁰⁶ Pb/ ²⁰⁸ Pb ^b | ²⁰⁶ Pb/ ²³⁸ U ^{cd} | ²⁰⁷ Pb/ ²³⁵ U ^{cd} | ²⁰⁷ Pb/ ²⁰⁶ Pb ^{cd} | ²⁰⁸ Pb/ ²³⁸ U | ²⁰⁷ Pb/ ²³⁵ U | ²⁰⁶ Pb/ ²⁰⁸ Pb | age (Ma) | age (Ma) | ρ ^e | disc ^f |
|---|--------|-----|-----|------------------|---|---|---|---|--|-------------------------------------|-------------------------------------|--------------------------------------|----------|----------|----------------|-------------------|
| | mg | ppm | ppm | ppm ^a | | | | | | | | | | | | % |
| KM-13 Chugwater anorthosite: 1435.95 ± 0.68 Ma (MSWD = 0.055) weighted average ²⁰⁷Pb/²⁰⁶Pb date | | | | | | | | | | | | | | | | |
| d-3 zrn sgl#2 anh | 0.380 | 168 | 48 | 0.05 | 49552 | 4.2 | 0.2483 (0.39) | 3.0981 (0.40) | 0.0905 (0.06) | 1430 | 1432 | 1436.0 ± 1.2 | 0.98 | 0.49 | | |
| d-3 zrn sgl#3 anh | 0.100 | 364 | 100 | 0.17 | 31235 | 5.3 | 0.2485 (0.35) | 3.1001 (0.36) | 0.0905 (0.06) | 1431 | 1433 | 1435.8 ± 1.2 | 0.99 | 0.40 | | |
| d-1 bdl 9gr | 0.250 | 83 | 19 | 0.02 | 61695 | 233.0 | 0.2481 (0.33) | 3.0953 (0.33) | 0.0905 (0.06) | 1428 | 1432 | 1436.1 ± 1.2 | 0.98 | 0.59 | | |
| KM-144 Chugwater anorthosite: 1435.7 ± 1.1 Ma (MSWD = 0.77) upper intercept four-point regression | | | | | | | | | | | | | | | | |
| d-2 zrn 4gr anh | 0.150 | 172 | 45 | 0.03 | 81383 | 7.3 | 0.2460 (0.35) | 3.0689 (0.35) | 0.0905 (0.06) | 1418 | 1425 | 1435.7 ± 1.2 | 0.98 | 1.40 | | |
| d-2 zrn#3 6gr anh | 0.097 | 102 | 27 | 0.51 | 2950 | 6.9 | 0.2457 (0.34) | 3.0623 (0.36) | 0.0904 (0.11) | 1416 | 1423 | 1434.2 ± 2.2 | 0.95 | 1.41 | | |
| d-1 zrn 6gr anh | 0.110 | 324 | 85 | 0.50 | 9396 | 6.7 | 0.2450 (0.35) | 3.0549 (0.36) | 0.0904 (0.06) | 1412 | 1421 | 1435.0 ± 1.2 | 0.98 | 1.76 | | |
| d-2 zrn#4 8gr anh | 0.056 | 217 | 53 | 0.42 | 7119 | 7.7 | 0.2307 (0.34) | 2.8746 (0.34) | 0.0904 (0.07) | 1338 | 1375 | 1433.4 ± 1.4 | 0.98 | 7.35 | | |
| KM-6 Chugwater anorthosite: 1435.21 ± 0.88 Ma (MSWD = 1.7) upper intercept three-point regression | | | | | | | | | | | | | | | | |
| d-1 bdl 20gr | 0.330 | 165 | 39 | 0.01 | 320160 | 838.0 | 0.2504 (0.43) | 3.1230 (0.43) | 0.0905 (0.06) | 1440 | 1438 | 1435.3 ± 1.2 | 0.99 | -0.41 | | |
| d-1 bdl#2 19gr | 0.224 | 161 | 56 | 0.12 | 20148 | 553.0 | 0.2480 (0.33) | 3.0936 (0.33) | 0.0905 (0.06) | 1428 | 1431 | 1435.4 ± 1.2 | 0.98 | 0.56 | | |
| d-2 bdl 12gr | 0.099 | 238 | 38 | 0.43 | 8217 | 544.0 | 0.2468 (0.33) | 3.0767 (0.33) | 0.0904 (0.07) | 1422 | 1427 | 1434.0 ± 1.3 | 0.98 | 0.92 | | |
| GM-148 Chugwater(?) anorthosite: 1435.25 ± 0.60 Ma (MSWD = 0.19) weighted average ²⁰⁷Pb/²⁰⁶Pb date | | | | | | | | | | | | | | | | |
| d-2 zrn 6gr euh | 0.557 | 89 | 23 | 0.11 | 11746 | 7.6 | 0.2484 (0.36) | 3.0974 (0.37) | 0.0904 (0.06) | 1430 | 1432 | 1434.9 ± 1.2 | 0.98 | 0.37 | | |
| m3 zrn 8gr euh | 0.134 | 588 | 158 | 0.62 | 13930 | 6.2 | 0.2484 (0.45) | 3.0990 (0.45) | 0.0905 (0.06) | 1430 | 1432 | 1435.5 ± 1.2 | 0.99 | 0.40 | | |
| d-3 zrn 9gr euh | 0.251 | 79 | 21 | 0.16 | 7113 | 5.6 | 0.2474 (0.34) | 3.0860 (0.34) | 0.0905 (0.07) | 1425 | 1429 | 1435.2 ± 1.3 | 0.98 | 0.77 | | |
| nm2 zrn 6gr frg | 0.260 | 127 | 33 | 0.04 | 48697 | 7.2 | 0.2471 (0.34) | 3.0820 (0.35) | 0.0905 (0.06) | 1423 | 1428 | 1435.4 ± 1.2 | 0.98 | 0.92 | | |
| BM-243 Snow Creek anorthosite | | | | | | | | | | | | | | | | |
| d-3 zrn 5gr anh | 0.116 | 147 | 38 | 0.06 | 33985 | 8.6 | 0.2487 (0.34) | 3.1050 (0.34) | 0.0906 (0.06) | 1432 | 1434 | 1437.4 ± 1.2 | 0.98 | 0.45 | | |
| d-1 zrn 3gr anh | 0.232 | 187 | 50 | 0.07 | 37256 | 6.7 | 0.2486 (0.35) | 3.1049 (0.36) | 0.0906 (0.06) | 1431 | 1434 | 1437.7 ± 1.2 | 0.99 | 0.49 | | |
| d-4 zrn 13gr anh | 0.209 | 150 | 40 | 0.05 | 47849 | 7.0 | 0.2483 (0.35) | 3.0994 (0.35) | 0.0905 (0.06) | 1430 | 1433 | 1436.7 ± 1.2 | 0.98 | 0.54 | | |
| d-4 zrn#2 17gr anh | 0.139 | 105 | 27 | 0.04 | 35351 | 7.9 | 0.2483 (0.34) | 3.1033 (0.34) | 0.0906 (0.06) | 1430 | 1434 | 1439.2 ± 1.2 | 0.98 | 0.74 | | |
| BM-5 Monzodiorite dike cross-cutting Snow Creek anorthosite | | | | | | | | | | | | | | | | |
| m3 zrn#2 10gr anh | 0.037 | 98 | 26 | 0.31 | 4570 | 8.0 | 0.2469 (0.37) | 3.0749 (0.40) | 0.0903 (0.13) | 1422 | 1426 | 1432.8 ± 2.4 | 0.98 | 0.82 | | |
| m3 zrn#3 9gr euh | 0.037 | 98 | 25 | 0.15 | 9527 | 7.9 | 0.2476 (0.37) | 3.0862 (0.38) | 0.0904 (0.08) | 1426 | 1429 | 1434.4 ± 1.6 | 0.95 | 0.66 | | |
| m3 zrn 17gr euh | 0.019 | 124 | 32 | 0.11 | 15954 | 8.1 | 0.2468 (0.45) | 3.1735 (0.46) | 0.0933 (0.12) | 1422 | 1451 | 1493.0 ± 2.2 | 0.97 | 5.30 | | |
| m2 zrn 11gr euh | 0.028 | 211 | 46 | 0.10 | 24944 | 7.5 | 0.2087 (0.35) | 2.6110 (0.36) | 0.0907 (0.10) | 1222 | 1304 | 1441.2 ± 1.9 | 0.96 | 16.70 | | |

Notes: mineral fraction; d_, nm_ represent angles of diamagnetic and paramagnetic susceptibility, respectively, on a barrier-style Frantz separator; zrn: zircon; bdl: baddeleyite; _gr: # of grains; euh: euhedral, anh: anhedral, frg: fragments. ^a Pb_c common Pb (ppm) corrected for laboratory blank.

^b Ratio corrected for blank and mass discrimination. ^c Radiogenic Pb in ratios; all values corrected for blank and mass discrimination. ^d Values in parentheses are 2σ errors in percent. ^e correlation coefficient ρ, ²⁰⁶Pb/²³⁸U versus ²⁰⁷Pb/²³⁵U error. ^f Percent discordant.

Zircon and baddeleyite dissolution and chemistry were adapted from methods developed by Krogh (1973) and Parrish *et al.* (1987). Aliquots of dissolved sample were spiked with a mixed ²⁰⁸Pb/²³⁵U tracer. The Pb and U samples were loaded onto single rhenium filaments with silica gel and graphite, respectively; isotopic compositions were measured in multicollector, static mode on a VG Sector mass spectrometer at the University of Wyoming in 1995. Mass-discrimination factors of 0.11 ± 0.06 ‰/amu for Pb and 0.0 ± 0.06 ‰/amu for U were determined by replicate analyses of NIST SRM 981 and U-500, respectively. Procedural blank was 10 pg Pb or less over the course of the study. Uranium blanks were consistently less than 1 pg. Concordia coordinates, intercepts, and uncertainties were calculated using PbDAT and ISOPLLOT programs (Ludwig 1988, 1991); initial Pb compositions were estimated by the Stacey & Kramers (1975) model. The decay constants used by PbDAT are those recommended by the I.U.G.S. Subcommittee on Geochronology (Steiger & Jäger 1977): 0.155125 × 10⁻⁹/yr for ²³⁸U, 0.98485 × 10⁻⁹/yr for ²³⁵U and present-day ²³⁸U/²³⁵U = 137.88. The ²⁰⁸Pb/²³⁵U tracer was calibrated against the MIT2 gravimetric standard and yielded a ²⁰⁸Pb/²³⁵U date of 419.26 ± 0.64 Ma for zircon standard R33 (²⁰⁷Pb/²³⁵U date of 420.11 ± 0.59 Ma), in good agreement with the ROM date for R33 (Black *et al.* 2004).

These concentrations are typical of Proterozoic massif anorthosites (*e.g.*, Higgins & van Breemen 1992, Owens *et al.* 1994, Scoates & Chamberlain 1995, 1997, 2003, Frost *et al.* 2000). Values of $^{206}\text{Pb}/^{204}\text{Pb}$ (corrected for fractionation, spike composition, and blank contribution) are high, ranging from 2,950 to 320,160 (Table 1), indicating low amounts of common Pb in zircon and baddeleyite.

Chugwater anorthosite (KM13)

Sample KM13 is a medium-grained, tabular anorthosite. This well-foliated rock is from King Mountain, the An3 unit of the Chugwater anorthosite (Lindsley *et al.* 2010). Stratigraphic reconstructions place it 8,860 m above the lowest exposed anorthosites in this layered anorthosite intrusion (Lindsley *et al.* 2010). The rock is composed of 93% plagioclase, which is deformed only locally, 2–3% ilmenite, and minor quartz, calcite, white mica and epidote. The U–Pb data from two anhedral single crystals of zircon and one nine-grain baddeleyite fraction are overlapping and concordant, with $^{207}\text{Pb}/^{206}\text{Pb}$ ages from 1435.8 to 1436.1 Ma (Fig. 2A). The weighted average $^{207}\text{Pb}/^{206}\text{Pb}$ age of 1436.0 ± 0.7 Ma is considered the best estimate for the age of crystallization of KM13.

Chugwater anorthosite (GM144)

Sample GM144 is a strongly deformed anorthosite located in the southeastern portion of the Chugwater anorthosite. It is composed of 96% plagioclase, which is mostly neoblastic. Relict large grains of plagioclase are kinked or bent. The sample contains minor late-stage calcite, white mica and chlorite. Four fractions of anhedral zircon were analyzed, each fraction containing between four and eight grains. The U–Pb data for three fractions are nearly concordant (1.4 to 1.8% discordant), whereas data from a fourth fraction are more discordant (7.4% discordant; Fig. 2B). An upper intercept age of 1435.7 ± 1.1 Ma was obtained from a linear regression of the four datasets, which is interpreted as a best estimate for the age of crystallization of GM144.

The Chugwater(?) anorthosite (GM148)

Sample GM148 comes from a small body of anorthosite that lies southeast of the Chugwater intrusion, and is less deformed than GM144. It is composed of 94% plagioclase, which is kinked and bent, but neoblasts are minor. Ferromagnesian minerals include subequal amounts of augite, orthopyroxene and inverted pigeonite. Ilmenite is more abundant than magnetite. Calcite, white mica and chlorite are minor. Four fractions, each composed of six to nine grains of euhedral zircon, were analyzed. The data from all fractions are nearly concordant (less than 1% discordant), and yield

$^{207}\text{Pb}/^{206}\text{Pb}$ ages of 1434.9 to 1435.5 Ma (Fig. 2C). The weighted average $^{207}\text{Pb}/^{206}\text{Pb}$ age, 1435.3 ± 0.6 Ma, is considered the best estimate for the age of crystallization of GM148.

The Chugwater gabbroanorthitic anorthosite (KM6)

Sample KM6 was taken from a leucogabbro layer in the An2 unit of the Chugwater intrusion located 4250 m above the base of the pluton (Lindsley *et al.* 2010). The rock is composed of 80% plagioclase, 5% orthopyroxene, 5% augite, 5% olivine, 2% biotite, 2% titaniferous magnetite with green spinel (hercynite) and 1% ilmenite. It is interpreted to be the product of mixing of leucotroctolitic magma with partially solidified Chugwater anorthosite (Lindsley *et al.* 2010). Three fractions of baddeleyite were analyzed from the sample, each fraction containing between 12 and 20 grains. The U–Pb data from these fractions include two concordant analyses and one nearly concordant analysis (0.92% discordant; Fig. 2D). A linear regression through these three datasets yields an upper intercept age of 1435.2 ± 0.9 Ma, interpreted as the age of crystallization of this sample.

The Chugwater anorthosite (BM136) from Scoates & Chamberlain (1995)

In addition to the ages reported above, an age acquired on a fifth sample of Chugwater anorthosite, BM136, is available (Scoates & Chamberlain 1995). This megacrystic anorthosite from the northern part of the Chugwater anorthosite (An1 unit) is from the 1404 m stratigraphic level, making it stratigraphically the lowest of the dated samples. It yielded abundant baddeleyite, but little zircon. The U–Pb data from four baddeleyite fractions gave a weighted average $^{207}\text{Pb}/^{206}\text{Pb}$ age of 1435.4 ± 0.5 Ma.

The Snow Creek anorthosite (BM243)

The Snow Creek anorthosite intrudes the Chugwater anorthosite to the south and the Poe Mountain anorthosite to the north. Sample BM243 is located west of the Strong Creek and Greaser intrusions. It is composed of 90% plagioclase, which is strongly bent and sutured and has a thin rim of mesoperthite. It contains augite, inverted pigeonite, ilmenite and quartz. Data from four fractions of anhedral zircon are nearly concordant (0.89 to 1.17% discordant), and yielded $^{207}\text{Pb}/^{206}\text{Pb}$ ages of 1436.7 to 1439.2 Ma (Fig. 2E). This range of $^{207}\text{Pb}/^{206}\text{Pb}$ ages exceeds analytical uncertainty, and a weighted average has no geological significance. We interpret the data as evidence for a small component of inherited zircon, and conclude that the youngest $^{207}\text{Pb}/^{206}\text{Pb}$ age of 1436.7 ± 1.2 Ma is a maximum age of crystallization. This interpretation is consistent

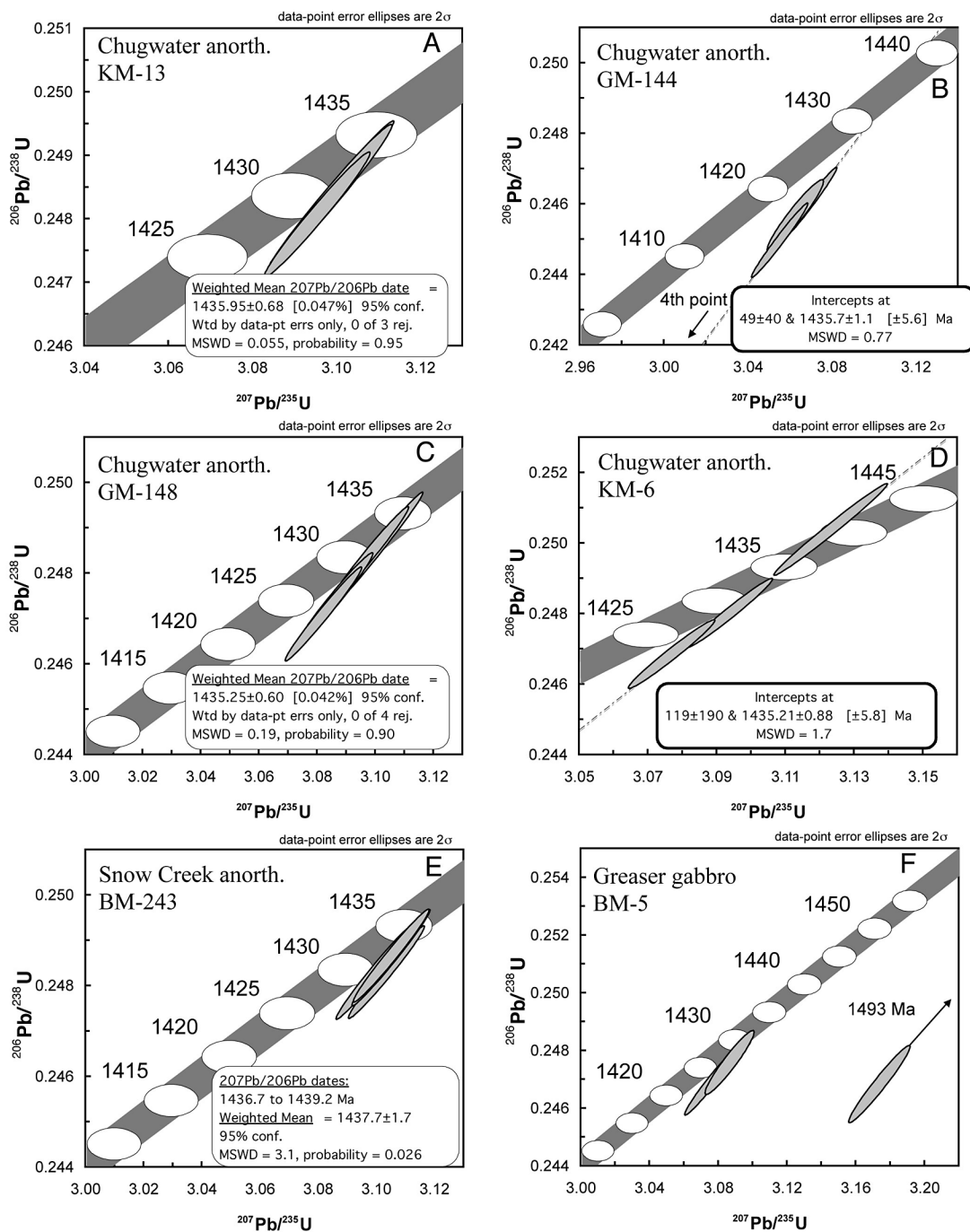


FIG. 2. U–Pb concordia diagrams for analyzed zircon and baddeleyite fractions from the Chugwater and Snow Creek anorthosites and the monzodiorite dike. The width of the concordia band represents effects of uncertainties in decay constants of the uranium isotopes.

with field evidence that the Snow Creek anorthosite is younger than the Chugwater and Poe Mountain anorthosites.

Monzodiorite dike (BM5) cutting the Strong Creek Complex, Chugwater anorthosite and Snow Creek anorthosite

This sample is from a monzodiorite dike 10 km long, 1–3 m wide that intrudes the Strong Creek complex, the Chugwater anorthosite and the Snow Creek anorthosite. On the basis of field relations, it is one of the youngest units in the central portion of the Laramie complex. The rock is fine grained, and composed of antiperthitic plagioclase, alkali feldspar, augite, olivine, Fe–Ti oxide, and apatite. Four fractions of zircon yielded $^{207}\text{Pb}/^{206}\text{Pb}$ ages of 1432.8 to 1493.0 Ma (Fig. 2F). Data from the fractions with the two youngest $^{207}\text{Pb}/^{206}\text{Pb}$ ages are less than 1% discordant. The older $^{207}\text{Pb}/^{206}\text{Pb}$ ages of the other fractions suggest the presence of an inherited component, consistent with Nd and Sr isotopic evidence of crustal contamination (Mitchell *et al.* 1996). We interpret the youngest $^{207}\text{Pb}/^{206}\text{Pb}$ age of 1432.8 ± 2.4 Ma as a maximum age for the intrusion of the monzodiorite dike.

Summary of geochronology

The five dated samples of Chugwater anorthosite are geographically and stratigraphically well distributed. They include both leucogabbro and anorthosite, both highly deformed and undeformed rocks, and samples where zircon is more abundant than baddeleyite as well as the converse. Despite this diversity, all ages from the Chugwater intrusion overlap within error. The weighted average age for these five samples is 1435.5 ± 0.3 Ma, with an MSWD of 0.78. The age of KM–6, interpreted as the result of mixing of troctolitic magma with an anorthositic crystal mush, is indistinguishable from the age of other Chugwater samples, implying that the troctolitic magma must have intruded and mixed very shortly after the anorthosite body was emplaced.

The individual determinations of age made for the Chugwater intrusion imply older ages than those of the Poe Mountain anorthosite, but they overlap within error. However, the weighted average age of the Chugwater intrusion (1435.5 ± 0.3 Ma) is older outside of error than the weighted average age of the Poe Mountain anorthosite samples (1434.4 ± 0.4 Ma; MSWD = 0.4). The age of the block of leucogabbroic anorthosite from within the Poe Mountain anorthosite is indistinguishable from the age of the Chugwater anorthosite. This xenolith contains iridescent plagioclase megacrysts (Scoates & Chamberlain 1995), as do the Chugwater anorthosites. However, Nd and Sr isotopic compositions of xenoliths in the Poe Mountain anorthosite contrast with the isotopic compositions of the Chugwater anorthosite. This suggests either that the Chugwater anorthosite was

more contaminated with Archean crust farther to the north where the block is located, or that the block was derived from a coeval, but different, intrusion than the Chugwater anorthosite.

Because zircon from the Snow Creek anorthosite contains inherited components, only a maximum age could be obtained by U–Pb dating. Therefore, although the Snow Creek intrusion is constrained to be the youngest intrusion of anorthosite on the basis of field relations, the absolute age could not be precisely determined. However, it is cut by the dike (BM–5), which has a maximum age of 1432.8 ± 2.4 Ma. The U–Pb data permit the interpretation that the dike is as young as the youngest pluton in the Laramie anorthosite complex, the Red Mountain pluton (1431.3 ± 1.4 Ma, Verts *et al.* 1996). This interpretation is compatible with field observations of monzodiorite dikes cutting all units of the Laramie anorthosite complex, but fewer cut the Red Mountain pluton than cut the other bodies. This date also constrains the age of the Snow Creek anorthosite to be older than the monzodiorite dike.

The U–Pb age determinations for LAC monzonitic plutons (Fig. 3) indicate that they intruded the anorthosites shortly after these were emplaced. Granite of the northern Sherman batholith slightly predates the anorthosites (1437.7 ± 2.4 Ma; Frost *et al.* 2002), whereas the Lincoln and Sherman granites of the southern Sherman batholith are younger (1430.6 ± 2.6 and 1433.0 ± 1.5 Ma; Frost *et al.* 1999). The entire LAC – Sherman batholith suite was emplaced over a period no greater than 12 million years, and possibly in as little as three million years (Fig. 3).

MINERALOGY, PETROLOGY AND GEOCHEMISTRY OF THE SNOW CREEK ANORTHOSITE

The mineralogy, petrology, and geochemistry of the Poe Mountain and Chugwater anorthosites have been described in other studies (see Lindsley *et al.* 2010, Scoates *et al.* 2010, and references therein). Below, we describe the mineralogy, petrology, and geochemistry of the Snow Creek anorthosite.

Snow Creek anorthosite: mineralogy

The Snow Creek anorthosite is distinguished from the Poe Mountain anorthosite by the absence of olivine and the presence of iridescent plagioclase and locally of quartz, especially in the western portion of the pluton, and from the Chugwater anorthosite by the absence of magnetite.

Plagioclase. Plagioclase from the Snow Creek anorthosite ranges in composition from An₄₇ to An₅₆ and shows a range of solid-state recrystallization. The earliest plagioclase is tabular and is black in hand specimen because it contains abundant needles of ilmenite. This plagioclase generally shows various degrees of deformation, including bending, with the development

of deformation twins. In areas of intense deformation, the plagioclase has been recrystallized to granoblastic grains that commonly exhibit *ca.* 120° triple grain interfaces. These neoblastic grains of plagioclase lack the ilmenite needles and appear grey to white in hand sample.

Pyroxene. Pyroxene occurs in all samples and forms typical “post-cumulus” textures in which grains enclose the margins of the tabular plagioclase. In strongly recrystallized rocks, pyroxene forms equant grains that are the same size as the associated plagioclase. Augite is found in all rocks, although in one sample (SR357), it is a highly exsolved subcalcic augite that would have been stable at temperatures of *ca.* 1100°C (Lindsley & Frost 1992). Highly exsolved inverted pigeonite is the most abundant low-Ca pyroxene, although the most

magnesian rocks contain orthopyroxene (Opx) instead. The X_{Fe} the low-Ca pyroxene ranges from 0.37 to 0.63 (Table 2).

Ilmenite. Most samples contain ilmenite, although in some samples, the amount is less than 0.1%. Ilmenite

TABLE 2. AVERAGE COMPOSITION OF MINERALS IN THE SNOW CREEK ANORTHOSITE

| | Augite | | | | Low-Ca pyroxene | | |
|--------------------------------|--------|--------|--------|--------|-----------------|--------|--------|
| | SR 345 | SR 357 | BM-210 | BM-223 | SR 345 | BM-210 | BM-223 |
| SiO ₂ wt. % | 51.19 | 49.59 | 51.08 | 50.42 | 51.75 | 49.84 | 50.20 |
| Al ₂ O ₃ | 2.62 | 1.55 | 0.20 | 0.41 | 1.36 | 0.18 | 0.25 |
| TiO ₂ | 0.70 | 1.46 | 0.93 | 1.72 | 0.30 | 0.71 | 0.90 |
| FeO | 9.67 | 19.05 | 15.79 | 14.80 | 22.45 | 30.97 | 26.31 |
| MnO | 0.21 | 0.40 | 0.32 | 0.31 | 0.39 | 0.60 | 0.56 |
| MgO | 13.74 | 13.68 | 10.22 | 11.62 | 21.66 | 13.54 | 16.91 |
| CaO | 21.24 | 13.63 | 20.57 | 19.52 | 1.37 | 3.39 | 3.58 |
| Na ₂ O | 0.31 | 0.17 | 0.14 | 0.22 | 0.03 | 0.02 | 0.02 |
| Total | 99.68 | 99.53 | 99.25 | 99.022 | 99.33 | 99.25 | 98.73 |
| Si <i>apfu</i> | 1.921 | 1.901 | 1.977 | 1.944 | 1.949 | 1.974 | 1.957 |
| Al | 0.116 | 0.070 | 0.006 | 0.012 | 0.060 | 0.005 | 0.007 |
| Ti | 0.020 | 0.054 | 0.042 | 0.078 | 0.009 | 0.033 | 0.041 |
| Fe | 0.303 | 0.626 | 0.511 | 0.477 | 0.707 | 1.026 | 0.858 |
| Mn | 0.007 | 0.014 | 0.011 | 0.010 | 0.013 | 0.020 | 0.019 |
| Mg | 0.768 | 0.783 | 0.590 | 0.668 | 1.217 | 0.800 | 0.983 |
| Ca | 0.854 | 0.557 | 0.853 | 0.807 | 0.055 | 1.144 | 1.150 |
| Na | 0.023 | 0.013 | 0.011 | 0.017 | 0.003 | 0.002 | 0.002 |
| Total | 4.012 | 4.017 | 4.001 | 4.013 | 4.013 | 4.005 | 4.016 |
| Wo | 0.443 | 0.283 | 0.437 | 0.413 | 0.028 | 0.073 | 0.075 |
| En | 0.399 | 0.398 | 0.302 | 0.342 | 0.615 | 0.406 | 0.494 |
| Fs | 0.158 | 0.318 | 0.262 | 0.245 | 0.357 | 0.521 | 0.431 |
| X(Fe) | 0.283 | 0.444 | 0.464 | 0.417 | 0.368 | 0.562 | 0.466 |
| N | 9 | 43 | * | * | 42 | * | * |

| | Ilmenite | | | | |
|--------------------------------|----------|-------|-------|-------|-------|
| | BM223 | BM249 | BM251 | SR345 | SR357 |
| TiO ₂ wt. % | 49.52 | 50.83 | 49.78 | 50.94 | 49.99 |
| FeO | 47.85 | 46.22 | 45.88 | 45.14 | 45.64 |
| MnO | 0.91 | 0.49 | 0.85 | 1.99 | 0.42 |
| Nb ₂ O ₅ | 0.06 | 0.02 | 0.01 | 0.04 | 0.01 |
| Total | 98.35 | 98.35 | 98.35 | 98.35 | 96.07 |
| Ti <i>apfu</i> | 0.954 | 0.989 | 0.978 | 0.985 | 0.988 |
| Fe ²⁺ | 0.935 | 0.978 | 0.960 | 0.942 | 0.979 |
| Fe ³⁺ | 0.091 | 0.022 | 0.043 | 0.029 | 0.024 |
| Mn | 0.020 | 0.011 | 0.019 | 0.043 | 0.009 |
| Nb | 0.000 | 0.000 | 0.000 | 0.000 | 0.000 |
| Ilm | 0.935 | 0.978 | 0.960 | 0.942 | 0.979 |
| Pyp | 0.020 | 0.011 | 0.019 | 0.043 | 0.009 |
| Hem | 0.045 | 0.011 | 0.022 | 0.015 | 0.012 |
| N | 9 | 13 | 7 | 9 | 10 |

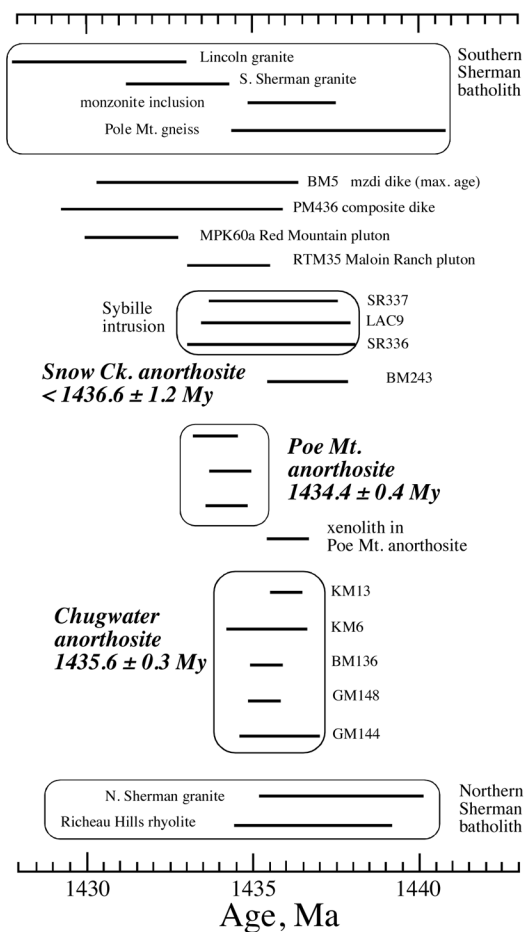


FIG. 3. Summary of geochronology for the Laramie anorthosite complex and the Sherman batholith. Data from this study, Frost *et al.* (1999, 2001), Scoates & Chamberlain (1995, 2003), Verts *et al.* (1996).

N: number of points involved in the average; *: analyses made by rastering a square 20 × 20 micrometers. Symbols: Wo wollastonite, En enstatite, Fs ferrosilite, Ilm ilmenite, Pyp pyrophanite, Hem hematite. Cation proportions in the pyroxenes were calculated on the basis of six atoms of oxygen. Cation proportions in the ilmenite were calculated on the basis of three atoms of oxygen.

contains less than 5 mole % of the Fe_2O_3 endmember (Table 2), similar to ilmenite from other labradorite anorthosites.

Biotite. Most samples contain small amounts of red-brown biotite. In some samples, it surrounds the ilmenite, in others it appears alone or in association with pyroxene.

Potassium feldspar. Orthoclase is present in most rocks. It occurs as small grains associated with recrystallized plagioclase in the highly deformed zones or as irregular blebs in tabular plagioclase. The textures suggest that the orthoclase formed by exsolution of the Or component of plagioclase during late-magmatic recrystallization.

Quartz. Quartz is present in many rocks. Like orthoclase, it occurs as small grains associated with recrystallized plagioclase. This texture suggests that the quartz may have formed from excess silica incorporated in plagioclase (Schwanke's molecule) during recrystallization of plagioclase. Quartz may also occur in zones of intense alteration, a texture suggesting that some quartz was produced as a by-product of low-T hydration reactions. In no rocks did we find textures indicating that quartz crystallized directly from the melt, so our interpretation is that these rocks were near but not at quartz-saturation.

Alteration. Few samples are pristine; most show some degree of low-temperature alteration. The most commonly observed alteration minerals are calcite and muscovite after plagioclase, chlorite and actinolite after pyroxene, and titanite and rutile after ilmenite.

Geochemistry

In this paper, we report results of 18 whole-rock analyses of samples from the Snow Creek anorthosite (Table 3), eight of which were reported in earlier papers (Mitchell *et al.* 1995, Scoates & Frost 1996). In those papers, however, it was not recognized that some of the rocks analyzed belong to the Snow Creek anorthosite; we include them here for completeness. The Snow Creek anorthosite has a wider spread in normative anorthite content than either the Poe Mountain or Chugwater anorthosites (Fig. 4). For most samples, the normative An of the other Snow Creek anorthosite samples are similar to that of the Chugwater anorthosite. This is not unexpected, as they both have iridescent plagioclase. However, four samples from the eastern part of the Snow Creek anorthosite have more sodic compositions. The easternmost portions of the Snow Creek anorthosite also range to more magnesian compositions than are found in the western portion, as indicated by the local occurrence of orthopyroxene. If this area is part of the same dome that is exposed in the west, it would be stratigraphically higher. The Poe Mountain and Chugwater anorthosites become more differentiated (and more ferroan) upward. A possible explanation for the lack of this trend in the Snow Creek

is that the eastern portion of the pluton intrudes the Poe Mountain anorthosite. It is likely that a transition zone exists between the Snow Creek anorthosite and Poe Mountain anorthosite where the Snow Creek has partially assimilated portions of the Poe Mountain anorthosite. This would explain why some portions of the Snow Creek have compositions that do not fit a simple differentiation trend and also why it is very difficult to locate the contact between the Snow Creek and Poe Mountain anorthositic plutons in the field.

Similar to other anorthositic rocks in the LAC (Scoates 1994, Lindsley *et al.* 2010), chondrite-normalized rare-earth-element (REE) patterns of the Snow Creek anorthosite have a positive Eu anomaly and are strongly depleted in heavy REE (Table 3, Fig. 5). The troctolite and leuconorite have higher REE abundances, with smaller positive Eu anomalies. The anorthositic rocks from the eastern body have lower abundances of REE with a larger Eu anomaly than those from the western body. The abundance of the REE is also positively correlated with P_2O_5 content, consistent with the interpretation that much of the REE in these rocks resides in the interstitial minerals, including apatite. We suggest that the intense deformation affecting the eastern rocks efficiently extracted intercumulus melt, causing the depletion in the REE. This is consistent with the observations of Lafrance *et al.* (1998), who proposed that the deformation observed in the anorthositic rocks of the LAC took place by fast grain-boundary migration, which was probably enhanced by the presence of a melt. The fact that the Eu content of all the samples from the Snow Creek anorthosite is about the same suggests that throughout the process, the bulk partition-coefficient for Eu was nearly 1.0.

ISOTOPE GEOCHEMISTRY

The Nd and Sr isotopic data from the Laramie anorthosite complex have been reported by Subbarayudu *et al.* (1975), Goldberg (1984), Geist *et al.* (1990), and Mitchell *et al.* (1995, 1996). Kolker *et al.* (1991), Scoates *et al.* (1996), and Anderson *et al.* (2003) focused on the isotopic characteristics of the monzonitic Maloin, Sybille, and Red Mountain intrusions, and Scoates & Frost (1996) described them for the Poe Mountain anorthosite. In this study, we report Nd and Sr isotopic compositions of the Chugwater and Snow Creek anorthosites (Table 4). In addition, we present results for one anorthosite sample from the eastern, undivided portion of the anorthositic area. Finally, to augment the isotopic dataset for monzodiorites from the Laramie anorthosite complex, we present data for three samples from the Sybille intrusion.

The Chugwater anorthosite

Samples from the Chugwater anorthosite exhibit a narrow range of initial Sr isotope ratios (0.70393

TABLE 3. GEOCHEMISTRY OF THE SNOW CREEK ANORTHOSITE

| Sample rock type | Western body | | | | | | | Eastern body | | | | | | | | | | |
|------------------------------------|----------------------------|----------------------------|----------------|-----------------|-----------------|-----------------|-----------------|----------------------------|----------------------------|----------------------------|----------------------------|---------------|-----------------------------|-----------------------------|-----------------|-----------------|-----------------|-----------------|
| | BM 30 ¹ 1 | BM 85 ¹ 2 | BM 243 2 | BM- 246 2 | BM- 250 2 | BM- 251 2 | SR- 350 2 | IG 11 ² 3 | IG 12 ² 2 | IG 21 ² 2 | IG 42 ² 2 | IG 44 2 | SR 297 ² 2 | SR 298 ² 2 | SR- 345 2 | SR- 347 2 | SR- 355 2 | SR- 357 2 |
| SiO ₂ wt% | 55.61 | 52.99 | 52.10 | 52.70 | 53.50 | 53.10 | 53.00 | 46.10 | 53.80 | 52.70 | 54.55 | 52.10 | 53.50 | 54.25 | 52.30 | 55.10 | 51.30 | 51.70 |
| TiO ₂ | 0.56 | 0.55 | 0.93 | 0.31 | 0.29 | 0.55 | 0.36 | 0.67 | 0.18 | 0.49 | 0.38 | 0.70 | 0.16 | 0.12 | 0.26 | 0.12 | 0.43 | 0.66 |
| Al ₂ O ₃ | 23.01 | 25.17 | 24.90 | 26.50 | 26.90 | 26.40 | 27.30 | 20.70 | 24.20 | 23.00 | 26.80 | 26.20 | 28.20 | 27.50 | 24.00 | 27.80 | 27.30 | 25.90 |
| Fe ₂ O ₃ (t) | 5.88 | 2.46 | 4.04 | 2.75 | 2.69 | 2.67 | 1.61 | 10.40 | 4.75 | 5.62 | 1.00 | 2.83 | 0.59 | 0.49 | 4.40 | 0.51 | 1.52 | 3.31 |
| MnO | 0.08 | 0.04 | 0.06 | 0.03 | 0.04 | 0.04 | 0.02 | 0.13 | 0.05 | 0.09 | 0.02 | 0.04 | 0.01 | 0.01 | 0.06 | 0.01 | 0.02 | 0.04 |
| MgO | 1.61 | 0.94 | 0.95 | 1.14 | 0.81 | 1.39 | 0.56 | 8.82 | 2.02 | 3.47 | 0.18 | 1.13 | 0.37 | 0.26 | 3.46 | 0.17 | 0.59 | 1.49 |
| CaO | 8.73 | 10.89 | 10.30 | 10.40 | 10.30 | 10.10 | 10.30 | 9.78 | 8.60 | 9.38 | 9.85 | 10.20 | 11.40 | 10.20 | 9.71 | 9.75 | 10.90 | 10.40 |
| Na ₂ O | 4.27 | 4.33 | 4.04 | 4.16 | 4.36 | 4.34 | 4.50 | 2.11 | 4.91 | 3.72 | 5.13 | 4.15 | 4.64 | 4.92 | 3.68 | 5.13 | 4.17 | 4.02 |
| K ₂ O | 1.11 | 0.76 | 0.87 | 0.62 | 0.62 | 0.63 | 0.73 | 0.50 | 1.08 | 0.76 | 0.88 | 0.75 | 0.62 | 1.04 | 0.45 | 0.78 | 0.62 | 0.66 |
| P ₂ O ₅ | 0.16 | 0.22 | 0.07 | 0.08 | 0.08 | 0.05 | 0.08 | 0.07 | 0.05 | 0.03 | 0.05 | 0.01 | 0.03 | 0.04 | 0.02 | 0.03 | 0.06 | 0.02 |
| LOI | 0.12 | 0.04 | 0.60 | 0.70 | 0.60 | 0.80 | 1.32 | 0.39 | 0.31 | 0.93 | 0.95 | 1.15 | 0.62 | 0.89 | 0.55 | 0.70 | 1.10 | 0.85 |
| Total | 101.14 | 98.39 | 98.86 | 99.39 | 99.99 | 100.07 | 99.78 | 99.67 | 99.95 | 100.19 | 99.79 | 99.26 | 100.14 | 99.72 | 98.89 | 100.10 | 98.01 | 99.05 |
| ap | 0.93 | 1.30 | 0.42 | 0.47 | 0.46 | 0.29 | 0.46 | 0.14 | 0.1 | 0.06 | 0.02 | 0.02 | 0.17 | 0.08 | 0.04 | 0.06 | 0.13 | 0.04 |
| ilm | 0.72 | 0.72 | 1.24 | 0.40 | 0.37 | 0.71 | 0.46 | 0.94 | 0.25 | 0.68 | 0.52 | 0.98 | 0.21 | 0.17 | 0.36 | 0.16 | 0.61 | 0.92 |
| or | 6.48 | 4.52 | 5.24 | 3.64 | 3.61 | 3.67 | 4.23 | 2.98 | 6.31 | 4.49 | 5.14 | 4.46 | 3.62 | 6.07 | 2.67 | 4.52 | 3.72 | 3.92 |
| ab | 37.90 | 39.13 | 36.98 | 37.16 | 38.54 | 38.40 | 39.60 | 19.07 | 43.58 | 33.42 | 45.58 | 37.5 | 41.12 | 42.86 | 33.21 | 45.2 | 37.98 | 36.33 |
| an | 39.88 | 47.31 | 48.16 | 51.54 | 50.66 | 49.96 | 51.10 | 45.78 | 40.33 | 43.84 | 47 | 50.86 | 53.59 | 49.26 | 47.89 | 47.28 | 54.46 | 51.02 |
| di | 1.10 | 2.65 | 1.48 | 0 | 0 | 0 | 0 | 2.07 | 1.21 | 2.02 | 0.82 | 0 | 0.84 | 0.36 | 0.32 | 0 | 0 | 0.63 |
| hy | 9.89 | 2.30 | 5.18 | 6.19 | 5.29 | 6.49 | 3.41 | 7.43 | 0.53 | 14.11 | 0.65 | 5.3 | 0.02 | 0 | 13.94 | 0.86 | 2.74 | 6.57 |
| ol | 0.00 | 0.00 | 0.00 | 0.00 | 0.00 | 0.00 | 0 | 19.95 | 6.96 | 0 | 0 | 0 | 0.67 | 0 | 0 | 0 | 0 | 0 |
| co | 0 | 0 | 0 | 0.15 | 0.20 | 0.26 | 0.45 | 0 | 0 | 0 | 0 | 0.04 | 0 | 0 | 0 | 0.92 | 0.11 | 0 |
| q | 3.09 | 2.05 | 1.31 | 0.45 | 0.87 | 0.21 | 0.30 | 0 | 0 | 0.49 | 0.02 | 0.39 | 0 | 0 | 0.87 | 0.91 | 0.02 | 0.04 |
| Ne | 0.00 | 0.00 | 0.00 | 0.00 | 0.00 | 0.00 | 0 | 0 | 0 | 0 | 0 | 0 | 0.46 | 0 | 0 | 0 | 0 | 0 |
| mt | 0 | 0 | 0 | 0 | 0 | 0 | 0 | 1.64 | 0.74 | 0.88 | 0.15 | 0.45 | 0.42 | 0.07 | 0.69 | 0.08 | 0.24 | 0.52 |
| pl (norm) | 84 | 91 | 90 | 92 | 93 | 92 | 95 | 68 | 90 | 82 | 98 | 93 | 98 | 98 | 85 | 97 | 96 | 91 |
| An (norm) | 0.47 | 0.52 | 0.53 | 0.56 | 0.55 | 0.54 | 0.54 | 0.68 | 0.45 | 0.48 | 0.48 | 0.55 | 0.55 | 0.50 | 0.57 | 0.49 | 0.57 | 0.56 |
| Mg# | 0.35 | 0.43 | 0.32 | 0.45 | 0.37 | 0.51 | 0.41 | 0.63 | 0.46 | 0.55 | 0.26 | 0.44 | 0.55 | 0.51 | 0.61 | 0.40 | 0.43 | 0.47 |
| Sc ppm | 15 | 3 | | 5 | 5 | 7 | 2 | 18 | 8 | 20 | 4 | | 6 | 4 | | 0.3 | 3 | 5 |
| V | 49 | 32 | | 29 | 25 | 81 | 26 | 57 | 6 | 70 | 15 | | 10 | 3 | | 3 | 25 | 50 |
| Cr | 11 | 7 | | 12 | 5 | 7 | 4 | 26 | 4 | 36 | 5 | | 4 | 3 | | 2 | 5 | 12 |
| Co | | | | 34 | 27 | 26 | 15 | 63 | 30 | 29 | 33 | | 20 | 13 | | 18 | 37 | 32 |
| Cu | 3 | 3 | | 5 | 10 | 3 | 3 | 9 | 38 | 10 | 4 | | 4 | 5 | | 3 | 7 | 7 |
| Zn | 89 | 25 | | 24 | 46 | 28 | 19 | 103 | 38 | 53 | 6 | | 9 | 11 | | 8 | 18 | 32 |
| Ga | | | | 25 | 30 | 27 | 26 | 20 | 24 | 23 | 31 | | 25 | 28 | | 35 | 24 | 26 |
| Rb | 8.34 | 6.21 | 12 | 3 | 4 | 4 | 7 | 3.9 | 4.3 | 2 | 4.2 | 20 | 2.96 | 7 | 12 | 3 | 4 | 3 |
| Sr | 527 | 718 | 765 | 718 | 781 | 269 | 418 | 1441 | 898 | 588 | 868 | 676 | 814 | 786 | 611 | 798 | 765 | 725 |
| Y | 23 | 8 | 12 | 6 | 6 | 3 | 3 | 9.6 | 1 | 2.8 | 0.5 | 2 | 1.6 | 1.4 | 3 | 0.5 | 2 | 2 |
| Zr | 108 | 17 | 86 | 23 | 26 | 11 | 19 | 58 | 16 | 40 | 36 | 20 | 24 | 19 | 21 | 2 | 22 | 5 |
| Nb | | | 11 | 3 | 3 | 2 | 2 | 1.7 | 0.5 | 1.2 | 0.7 | 2 | 1 | 0.1 | 2 | 0.2 | 2 | 1 |
| Ba | 560 | 357 | 416 | 319 | 419 | 391 | 311 | 265 | 613 | 389 | 565 | 448 | 312 | 439 | 246 | 565 | 302 | 289 |
| Sr/Ba | 0.94 | 2.01 | 1.84 | 2.25 | 1.86 | 0.69 | 1.34 | 5.44 | 1.46 | 1.51 | 1.54 | 1.51 | 2.61 | 1.79 | 2.48 | 1.41 | 2.53 | 2.51 |
| La | 47.60 | 8.32 | 9.93 | 9.12 | 11.76 | 8.74 | 9.76 | 5.93 | 3.40 | 2.93 | 3.88 | | 3.83 | 4.05 | | 3.64 | 5.00 | 4.69 |
| Ce | 86.30 | 17.10 | 17.93 | 17.81 | 21.20 | 14.77 | 16.21 | 14.37 | 6.65 | 5.76 | 6.06 | | 7.61 | 6.28 | | 5.80 | 9.39 | 7.36 |
| Nd | 37.00 | 8.48 | 8.65 | 8.38 | 9.09 | 5.61 | 7.22 | 9.38 | 2.66 | 2.83 | 2.38 | | 3.20 | 2.63 | | 2.28 | 4.54 | 3.06 |
| Sm | 6.70 | 1.52 | 1.81 | 1.58 | 1.62 | 0.86 | 1.23 | 1.93 | 0.44 | 0.56 | 0.40 | | 0.60 | 0.39 | | 0.28 | 0.80 | 0.46 |
| Eu | 2.12 | 1.79 | 1.86 | 1.55 | 1.94 | 2.45 | 1.84 | 1.02 | 1.80 | 1.34 | 2.29 | | 1.53 | 1.54 | | 1.93 | 1.51 | 1.72 |
| Gd | 5.42 | 1.66 | 2.29 | 1.43 | 1.46 | 0.74 | 1.03 | 2.12 | 0.42 | 0.60 | 0.24 | | 0.50 | 0.24 | | 0.18 | 0.65 | 0.41 |
| Dy | 4.28 | 1.25 | 1.92 | 1.18 | 1.18 | 0.61 | 0.69 | 1.78 | 0.20 | 0.45 | 0.14 | | 0.34 | 0.14 | | 0.10 | 0.47 | 0.34 |
| Er | 1.87 | 0.55 | 0.87 | 0.58 | 0.57 | 0.30 | 0.31 | 0.78 | 0.09 | 0.23 | 0.08 | | 0.14 | 0.07 | | 0.04 | 0.21 | 0.17 |
| Yb | 1.59 | 0.48 | 0.67 | 0.50 | 0.51 | 0.25 | 0.23 | 0.66 | 0.09 | 0.25 | 0.06 | | 0.13 | 0.06 | | 0.02 | 0.18 | 0.15 |
| Lu | 0.23 | 0.98 | 1.08 | 0.08 | 0.08 | 0.04 | 0.04 | 0.10 | 0.01 | 0.04 | 0.01 | | 0.02 | 0.01 | | 0.00 | 0.03 | 0.03 |

1: analytical data reported by Mitchell *et al.* (1995); 2: analytical results reported by Scoates (1994). Rock types: 1: leuconorite, 2: anorthosite, 3: troctolite.

to 0.70445), but a large range in initial ϵ_{Nd} (+2.4 to -1.5) (Fig. 6). The samples include anorthosite *sensu stricto* and anorthositic rocks with 80–90% plagioclase,

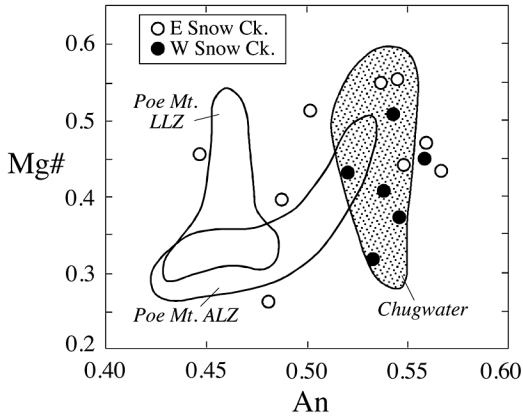


FIG. 4. Mg# versus normative An for anorthosites of the Snow Creek anorthosite compared to fields for data from Chugwater (Lindsley *et al.* 2010) and Poe Mountain anorthosites (Scoates 1994). ALZ: anorthositic layered zone, LLZ: leucogabbroic layered zone.

including gabbroic, gabbronoritic, and troctolitic anorthosites. The more mafic anorthositic rocks have been interpreted as mixtures of troctolitic magmas with partially crystallized anorthosite in a pluton that consists of three main layers, each of which are anorthositic at the base and gabbroic at the top. Fractionation is suggested by upward increases in incompatible elements (Lindsley *et al.* 2010). According to this interpretation, at least three different magmas were involved in the production of the Chugwater anorthosite body: an anorthosite-producing magma, and at least two leucotroctolitic magmas.

The Chugwater anorthosite includes samples with the most strongly positive initial ϵ_{Nd} of any samples, regardless of rock type, anywhere in the Laramie anorthosite complex. Because crustal assimilation will result in less radiogenic initial ϵ_{Nd} (lower values), the parent magma for Chugwater anorthosite must have had initial ϵ_{Nd} of +2.4 or higher. The sample with initial ϵ_{Nd} of +2.4 (BM137) is the anorthosite from the lowest stratigraphic level in the Chugwater anorthosite. The anorthosite sample from the highest stratigraphic level (KM13) has the most strongly negative initial ϵ_{Nd} of -1.3, and samples from intermediate levels have intermediate initial ϵ_{Nd} values. This range of initial ϵ_{Nd} suggests that crustal assimilation occurred at the level of emplacement, not during magma ascent, and that

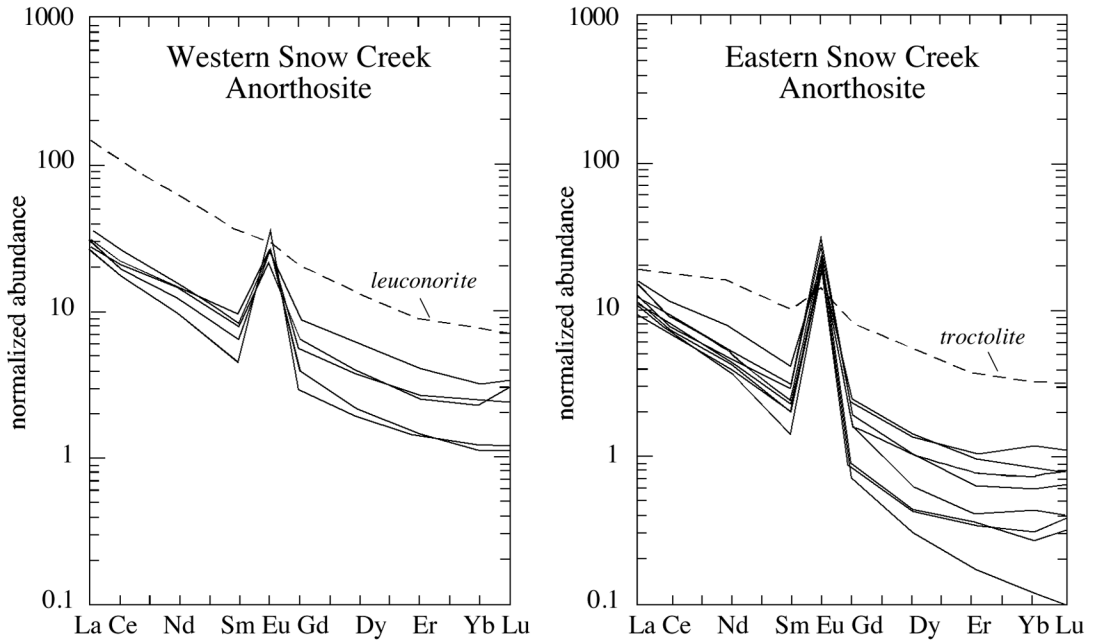


FIG. 5. Chondrite-normalized rare-earth-element plots for the western and eastern Snow Creek anorthosite. The lower abundances of rare-earth elements and more pronounced Eu anomalies in the western Snow Creek samples are interpreted to reflect more efficient expulsion of trapped liquid from the eastern Snow Creek anorthosite late in its crystallization history. Chondrite-normalized values from Wakita *et al.* (1971).

magmas in the upper portions of the body nearest the roof rocks were the most strongly contaminated.

The gabbroic and troctolitic anorthosites vary in initial ϵ_{Nd} from +0.9 to 0.1. Again, assuming that the parent magma becomes less radiogenic with crustal assimilation, then the parent troctolitic magma had initial ϵ_{Nd} of +0.9 or higher. This value is slightly lower than the least contaminated of the LAC high-Al gabbros (+2.0; Mitchell *et al.* 1995). The high-Al gabbros were interpreted as mantle-derived magmas parental to LAC anorthosite, and these least-contaminated samples are from the southern LAC. The high-Al gabbros have a lower initial $^{87}Sr/^{86}Sr$ value than the gabbroic and troctolitic anorthosites of the Chugwater anorthosite.

The sample of undivided anorthosite located east of several Laramide faults (Fig. 1) consists of well-laminated, medium-grained (crystals 2–3 cm across, 2–3 mm thick) tabular anorthosite. We analyzed the Nd and Sr isotopic compositions of this sample (95DR2) because it closely resembles King Mountain Anorthosite, the most distinctive unit of the Chugwater anorthosite. Its relatively high initial ϵ_{Nd} of +0.7 and its initial Sr isotopic ratio of 0.70435 place it within the field of Chugwater anorthosites. In addition, a troctolite and a gabbro sample from this area, 95IG2 and 3, also have similar Sr and Nd isotopic characteristics to Chugwater anorthosite (initial $^{87}Sr/^{86}Sr$ and ϵ_{Nd} equal to 0.70443 and 1.43, and 0.70421 and 0.11, respectively; Frost *et al.* 2001). If this portion of the Laramie anorthosite complex is part of the Chugwater anorthosite, then Laramide faulting has translated the eastern portions of the anorthosite area 15 km or more to the north, or this sample is part of what was originally a much more extensive Chugwater intrusion.

Sample GM146 is an inclusion of white, fine-grained anorthosite in Chugwater anorthosite. It and a number of other inclusions found in the central Chugwater anorthosite and along the contact with the Maloin Ranch pluton are characterized by plagioclase with a higher anorthite content and are geochemically distinct in many other ways (Lindsley *et al.* 2010). The higher initial $^{87}Sr/^{86}Sr$ value of this sample distinguishes it from the Chugwater anorthosite samples as well. This inclusion is interpreted as a block of an older body of anorthosite that is present at depth beneath the southern LAC, inclusions of which were brought up to the present level of exposure as Chugwater anorthosite magmas ascended through this body. The older anorthosite could be as old as 1.76 Ga, when the Horse Creek anorthosite was emplaced approximately 5 km south of the southern limit of the Chugwater anorthosite (Scoates & Chamberlain 1997, Frost *et al.* 2000).

The Snow Creek anorthosite

There are nine Nd and Sr isotopic analyses of rocks from the Snow Creek anorthosite (Table 4), including some previously published analyses of samples that

are now recognized as part of the Snow Creek anorthosite. Like the Chugwater anorthosite, the range of initial $^{87}Sr/^{86}Sr$ ratios of the Snow Creek anorthosite is relatively narrow, whereas the variation in initial ϵ_{Nd} is large. However, the Chugwater and Snow Creek anorthosites have distinct Sr and Nd isotopic compositions. The Snow Creek anorthosite has more radiogenic $^{87}Sr/^{86}Sr$ values, 0.7051–0.7056, and more negative ϵ_{Nd} , from –1.3 to –4.7. These isotopic compositions are consistent with a larger amount of crustal contamination in the Snow Creek anorthosite than in the Chugwater anorthosite. Alternatively (and more likely), a greater proportion of Archean contaminant may have affected the Snow Creek anorthosite, whereas the Chugwater anorthosite may have passed through primarily Proterozoic crust, which would have resulted in less extreme Nd and Sr isotopic compositions.

Ferrodioritic rocks

Included on Table 4 are three additional analyses of ferrodioritic rocks collected from the vicinity of the Sybille–Poe boundary to augment the analyses of Mitchell *et al.* (1996). These samples are among the ferrodiorites with the highest initial $^{87}Sr/^{86}Sr$ ratios, and they have relatively low initial ϵ_{Nd} . This is consistent with the geographic correlation observed by Mitchell *et al.* (1996), whereby the ferrodiorites located closest to Archean outcrops along the northern boundary of the LAC have the highest initial $^{87}Sr/^{86}Sr$ values. Mitchell *et al.* interpreted this as reflecting a greater amount of Archean assimilant in magmas intruded farther north. The isotopic compositions of the three samples presented in Table 4 imply a larger degree of crustal

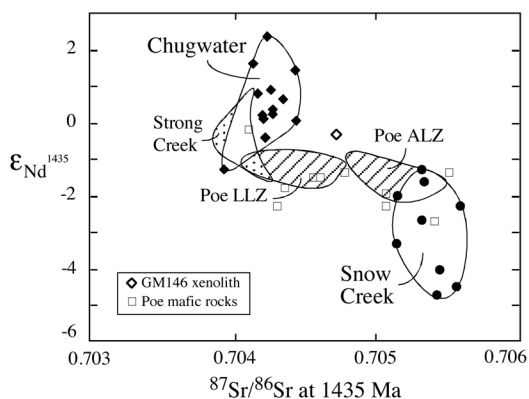


FIG. 6. Initial Sr and Nd isotopic compositions of LAC anorthosites, calculated for 1435 Ma. Squares: mafic rocks associated with the Poe Mountain anorthosite. Open diamond is sample GM146, a block of more calcic anorthosite found in the Chugwater pluton. Data from this study, Scoates & Frost (1996), and Mitchell *et al.* (1995).

TABLE 4. Nd AND Sr ISOTOPIC DATA FOR THE CHUGWATER AND SNOW CREEK ANORTHOSITES

| Sample, lithology | Rb ppm | Sr ppm | ⁸⁷ Rb/ ⁸⁶ Sr | ⁸⁷ Sr/ ⁸⁶ Sr | Initial Sr | Sm ppm | Nd ppm | ¹⁴⁷ Sm/ ¹⁴⁴ Nd | ¹⁴³ Nd/ ¹⁴⁴ Nd | Initial Nd | ε _{Nd} |
|--------------------------------|-----------|-----------|---------------------------------------|---------------------------------------|---------------|-----------|-----------|---|---|------------|-----------------|
| Chugwater anorthosite | | | | | | | | | | | |
| BM137 anorthosite | 1.60 | 916 | 0.0051 | 0.70434 | 0.70423 | 0.30 | 1.86 | 0.0983 | 0.511847 | 0.510921 | 2.7 |
| BM137 replicate | 1.57 | 1012 | 0.0045 | 0.70433 | 0.70424 | 0.32 | 2.18 | 0.0894 | 0.511732 | 0.510890 | 2.1 |
| BM146 anorthosite | 2.18 | 880 | 0.0072 | 0.70442 | 0.70428 | 0.53 | 2.99 | 0.1076 | 0.511813 | 0.510800 | 0.3 |
| BM160 leucotroctolite | 3.73 | 724 | 0.0149 | 0.70457 | 0.70426 | 1.51 | 7.32 | 0.1245 | 0.512004 | 0.510831 | 0.9 |
| KM6 gabbroanorthic anorthosite | 3.50 | 894 | 0.0113 | 0.70443 | 0.70420 | 0.48 | 2.73 | 0.1060 | 0.511792 | 0.510793 | 0.2 |
| RTM74 gabbroic anorthosite | 3.68 | 823 | 0.0129 | 0.70443 | 0.70417 | 0.88 | 4.95 | 0.1077 | 0.511840 | 0.510825 | 0.8 |
| KM13 anorthosite of King Mtn. | 7.38 | 859 | 0.0248 | 0.70445 | 0.70393 | 1.89 | 9.81 | 0.1168 | 0.511820 | 0.510720 | -1.3 |
| GM141 mafic anorthosite | 4.62 | 877 | 0.0152 | 0.70476 | 0.70445 | 0.96 | 4.68 | 0.1240 | 0.511953 | 0.510785 | 0.1 |
| GM148 anorthosite | 6.19 | 1016 | 0.0176 | 0.70450 | 0.70414 | 1.74 | 9.92 | 0.1062 | 0.511867 | 0.510866 | 1.6 |
| Anorthosite – undivided | | | | | | | | | | | |
| ^95DR2 anorthosite | 11.67 | 980 | 0.0345 | 0.70505 | 0.70435 | 4.70 | 28.37 | 0.1002 | 0.511763 | 0.510815 | 0.7 |
| ^95IG2 troctolite | 2.92 | 602 | 0.0140 | 0.70471 | 0.70443 | 0.78 | 5.28 | 0.0898 | 0.511704 | 0.510854 | 1.4 |
| ^95IG3 gabbro | 1.86 | 558 | 0.0097 | 0.70440 | 0.70421 | 0.54 | 1.96 | 0.1671 | 0.512365 | 0.510784 | 0.1 |
| GM146 anorthosite xenolith | 3.33 | 809 | 0.0119 | 0.70496 | 0.70471 | 0.73 | 6.21 | 0.0708 | 0.511434 | 0.510768 | -0.3 |
| Snow Creek anorthosite | | | | | | | | | | | |
| BM243 anorthosite | 11.72 | 765 | 0.0443 | 0.70650 | 0.70557 | 2.43 | 13.73 | 0.1071 | 0.511679 | 0.510670 | -2.2 |
| BM246 anorthosite | 2.60 | 718 | 0.0105 | 0.70553 | 0.70531 | 1.62 | 9.14 | 0.1073 | 0.511658 | 0.510647 | -2.7 |
| *BM30 leuconorite | 8.34 | 527 | 0.0457 | 0.70649 | 0.70555 | 5.95 | 32.20 | 0.1118 | 0.511610 | 0.510560 | -4.5 |
| *BM85 anorthosite | 6.21 | 718 | 0.0250 | 0.70594 | 0.70542 | 1.41 | 7.23 | 0.1179 | 0.511660 | 0.510540 | -4.7 |
| IG42 anorthosite | 4.16 | 868 | 0.0139 | 0.70568 | 0.70539 | 0.40 | 2.38 | 0.1018 | 0.511513 | 0.510554 | -4.5 |
| *SR357 anorthosite | 2.60 | 725 | 0.0104 | 0.70552 | 0.70531 | 0.38 | 2.65 | 0.0878 | 0.511547 | 0.510720 | -1.3 |
| *IG11 troctolite | 7.91 | 1441 | 0.0159 | 0.70546 | 0.70513 | 0.75 | 4.42 | 0.1022 | 0.511580 | 0.510620 | -3.3 |
| #SR298 anorthosite | 7.02 | 786 | 0.0258 | 0.70567 | 0.70514 | 0.25 | 1.74 | 0.0867 | 0.511501 | 0.510680 | -2.0 |
| #IG21 anorthosite | 2.00 | 588 | 0.0098 | 0.70553 | 0.70533 | 0.48 | 2.40 | 0.1201 | 0.511834 | 0.510700 | -1.6 |
| #SR297 anorthosite | 2.96 | 814 | 0.0105 | 0.70565 | 0.70543 | 0.51 | 2.93 | 0.1050 | 0.511568 | 0.510580 | -4.0 |
| Sybillie monzodiorites | | | | | | | | | | | |
| GR315 monzodiorite | 11.71 | 457 | 0.0742 | 0.71023 | 0.70870 | 14.49 | 70.50 | 0.1243 | 0.511852 | 0.510681 | -2.0 |
| PM103 monzodiorite | 21.38 | 504 | 0.1228 | 0.71247 | 0.70994 | 12.14 | 59.87 | 0.1226 | 0.511888 | 0.510732 | -1.0 |
| LAC 6b monzodiorite | 14.56 | 415 | 0.1016 | 0.71317 | 0.71108 | 14.76 | 73.07 | 0.1221 | 0.511861 | 0.510711 | -1.4 |

Analytical details: ~80 mg of sample were dissolved in HF–HNO₃. After conversion to chlorides, 1/3 of the sample was spiked with ⁸⁷Rb, ⁸⁴Sr, ¹⁴⁹Sm, and ¹⁴⁶Nd. Rubidium, Sr, and the REE were separated by conventional cation-exchange procedures. Samarium and Nd were further separated in di-ethyl-hexyl orthophosphoric acid columns. All isotopic measurements were made on a VG Sector multi-collector mass spectrometer at the University of Wyoming. An average ⁸⁷Sr/⁸⁶Sr value of 0.710246 ± 23 (2 sigma) was measured for NBS987 Sr, and an average ¹⁴³Nd/¹⁴⁴Nd value of 0.511846 ± 11 (2 sigma) normalized to ¹⁴⁶Nd/¹⁴⁴Nd = 0.7219 was measured for the La Jolla Nd standard. The uncertainties in Rb, Sr, Sm and Nd concentrations is ±2% of the measured value; the uncertainty in initial ε_{Nd} is ±0.5 epsilon units. * Previously published in Mitchell *et al.* (1995). # Previously published in Scoates & Frost (1996). ^ Previously published in Frost *et al.* (2002).

assimilation than the Sybillie monzosyenite they intrude. Therefore, these particular ferrodiorites cannot be parental melts to Sybillie, but may represent a different generation of ferrodiorite formed by a similar process.

DISCUSSION

Evidence for crustal assimilation in anorthosite plutons of the LAC

The Poe Mountain, Chugwater, and Snow Creek anorthosite plutons were emplaced in close succession.

The Chugwater anorthosite is marginally the oldest, emplaced at 1435.5 Ma, closely followed by the Poe Mountain anorthosite. The Snow Creek is constrained to be the youngest intrusion of anorthosite on the basis of field relations, and must be older than the ≤1432.8 Ma cross-cutting monzodiorite dike. Geochemical evidence for interaction of Snow Creek magmas with residual liquid remaining in the Poe Mountain anorthosite pluton described above is further evidence that the plutons were emplaced close together in time as well as in space. Doming and high-temperature deformation affected all three plutons, evidently while there was still

residual melt present. The continuity of the layering that is well-developed in the Poe Mountain and Chugwater anorthosites (Fig. 1; Scoates 1994, Lindsley *et al.* 2010) suggests that the doming affected both of these plutons together. Whether this deformation took place during or after emplacement of the Snow Creek anorthosite is less certain because of the relatively poor exposures of this youngest anorthosite pluton. In any case, the three plutons intruded each other within a relatively short period of approximately 1 to 5 million years. The tectonic environment and conditions of magma generation in this location were unlikely to change in this short time interval. It therefore seems likely that these plutons shared a common parental magma.

Despite their nearly simultaneous emplacement, each of the LAC anorthosite plutons displays a distinctive mineral assemblage. The Poe Mountain anorthosite is characterized by olivine, augite, low Ca-pyroxene, ilmenite and magnetite, and plagioclase in the range An_{43–53}. The Chugwater anorthosite generally contains no olivine, but is composed of augite, low Ca-pyroxene, ilmenite and magnetite, and plagioclase in the range An_{50–56}; it locally contains quartz. The Snow Creek anorthosite is characterized by a lack of olivine and magnetite and the presence of iridescent plagioclase with An₄₇ to An₅₆. It is commonly contains quartz, particularly in the western portion.

Isotopic evidence suggests that differences in mineralogy between the plutons may be related to varying amounts of crustal assimilation. Two lines of evidence suggest that the quartz-bearing Snow Creek pluton assimilated the most strongly felsic crust. First, the Snow Creek anorthosite is the only pluton that exhibits an inherited component in its zircon. Four fractions of zircon yielded ²⁰⁷Pb/²⁰⁶Pb ages from 1436.7 to 1439.2 (Fig. 2e), all of which exceed the maximum age of the pluton of 1434.4 ± 0.4 Ma represented by the age of the Poe Mountain anorthosite it intrudes. Second, the initial ε_{Nd} are the most strongly negative of the three plutons (Fig. 6), again suggesting assimilation of Precambrian crust. The Snow Creek anorthosite lies along the trace of the south-dipping suture between Archean and Proterozoic crust; hence, the crustal assimilant is constrained to be almost entirely Archean in age.

The Poe Mountain anorthosite, which lies north of the trace of the south-dipping Archean–Proterozoic suture, has less strongly negative initial ε_{Nd} than the Snow Creek anorthosite (Fig. 6). As only Archean crust was available as an assimilant to the Poe Mountain anorthosite, it must have experienced less contamination than the Snow Creek anorthosite. Simple bulk-assimilation models suggest no more than 3% Archean component in Poe Mountain anorthosites compared to up to 10% in Snow Creek (Scoates & Frost 1996). The presence of olivine in Poe Mountain anorthosite is consistent with this lesser extent of contamination.

The Chugwater anorthosite intrudes Proterozoic crust at the current level of exposure, and Archean

crust is present at depth. Its more radiogenic initial ε_{Nd} compared to the other plutons (Fig. 6) probably reflects the assimilation of Proterozoic crust with less strongly negative ε_{Nd} than the Archean rocks. This interpretation is consistent with the relatively high activity of silica in the Chugwater anorthosite (0.7 to 1.0; Lindsley *et al.* 2010); contamination of a mantle-derived magma would raise the silica activity above that for olivine saturation (0.67–0.70; Lindsley *et al.* 2010).

The relationship of oxygen fugacity and silica activity in anorthosite plutons

The effects of crustal assimilation in the anorthositic plutons of the LAC are reflected in the mineral assemblages of these rocks. This may be understood from silica-dependent equilibria relating the relations among Fe–Ti oxides, orthopyroxene, olivine, and quartz (Table 5). The first five of the reactions in Table 5 are QUIIF-related reactions tabulated by Lindsley & Frost (1992). The second five are very similar to the first five; in fact, some have the same stoichiometry as a QUIIF-related equilibrium. We have written them as separate reactions to emphasize that in these, unlike the QUIIF-related equilibria, silica is a mobile component. We show how these reactions are related in Figure 7, as calculated with the QUILF program of Andersen *et al.* (1993). The stability of Opx + Mgt + Ilm on this diagram is bounded at low oxygen fugacities by the stability of olivine (OPUIO) and at high *f*(O₂) by the stability of quartz (QUIIOp). In our

TABLE 5. SILICA- OR OXYGEN-DEPENDENT EQUILIBRIA BETWEEN SILICATES AND OXIDES

| | |
|--|----------|
| 4 Fe ₃ O ₄ + O ₂ = 6 Fe ₂ O ₃ Mgt Hem | (MH) |
| 6 FeSiO ₃ + O ₂ = 2 Fe ₃ O ₄ + 6 SiO ₂ Opx Mgt Qtz | (OpMQ) |
| 4 FeSiO ₃ + O ₂ = 2 Fe ₂ O ₃ + 4 SiO ₂ Opx Hem Qtz | (OpHQ) |
| SiO ₂ + Fe ₂ TiO ₄ = FeTiO ₃ + FeSiO ₃ Qtz Usp Ilm Opx | (QUIIOp) |
| FeSiO ₃ + Fe ₂ TiO ₄ = FeTiO ₃ + Fe ₂ SiO ₄ Opx Usp Ilm Ol | (OpUIIO) |
| Fe ₂ SiO ₄ + SiO ₂ = Fe ₂ Si ₂ O ₆ Ol melt Opx | (1) |
| 2 Fe ₃ O ₄ + 6 SiO ₂ = 3 FeSiO ₃ + O ₂ Mgt melt Opx | (2) |
| 2 Fe ₂ O ₃ + 4 SiO ₂ = 2 FeSiO ₃ + O ₂ in Ilm melt Opx | (3) |
| 2 Fe ₂ TiO ₄ + 2 SiO ₂ = 2 FeTiO ₃ + FeSiO ₃ in Mgt melt Ilm Opx | (4) |
| 2 Fe ₃ O ₄ + 2 SiO ₂ = 2 Fe ₂ O ₃ + FeSiO ₃ Mgt melt in Ilm Opx | (5) |

calculations, we assumed a temperature of 1000°C, a pressure of 3000 bars, and saturation of orthopyroxene with a calcic phase. We chose a compositional range at moderate values of μ_{FeMg} where olivine + quartz do not coexist, because this is the range represented by most anorthositic. On this figure, we do not specify where pigeonite is stable relative to orthopyroxene + augite for two reasons. First, the difference between the pigeonite-saturated and orthopyroxene-saturated curves is minimal (see Lindsley & Frost 1992). Second, pigeonite stability is clearly a function of temperature, and therefore it is reasonable to expect that some plutons will contain pigeonite, whereas other plutons with similar bulk-compositions may have orthopyroxene. It is important to recognize that this figure (and others like it in the text) is best used as a topology, rather than a phase diagram. This is because it is unlikely that rocks crystallizing an orthopyroxene with X_{Mg} ranging from 0.2 to 0.7 would crystallize at the same temperature. Whereas 1000°C may be a reasonable temperature for the iron-rich rocks, a temperature closer to 1100°C is

likely for the magnesian end. Most of the equilibria on the figure, especially OpUIIO and QUIIOp slide to more oxidizing conditions with decreasing temperature; thus any parameter, such as the relative fugacity of oxygen in a rock containing a fixed orthopyroxene or ilmenite composition will be valid only for the pressure and temperature at which the figure was calculated. Despite this shortcoming, the topological relations we describe below that are inferred from the figure are valid, regardless of the temperature of equilibration for the rocks involved.

It is well known that olivine is a sink for silica and, as long as olivine is present in a magma, silica activity will be kept fixed by reaction (1) (Table 5). It is less obvious that in a rock containing Fe–Ti oxide minerals, oxygen fugacity is directly related to silica activity. This relationship is clear from the stoichiometry of reactions (2) and (3), but it is not simple to quantify this relationship, however, because oxygen fugacity is a function of $\mu_{\text{FeMg}_{-1}}$ in the silicates and $\mu_{\text{FeTi}_{-1}}$ in the oxide minerals, both of which are sensitive to variations in silica activity.

As long as olivine is present in the magma, silica will be consumed by reaction (1) to produce orthopyroxene. However, once olivine has been depleted, silica will still be consumed by reactions (2), (3), (4) and (5). The stoichiometry of reactions (4) and (5), which are closed with respect to oxygen, indicates that each mole of magnetite in the rock has the potential to consume one mole of silica. To quantify how this affects the composition of the silicates, let us consider a rock with the assemblage Opx–mgt–ilm and trace amounts of olivine (*i.e.*, sitting on the OpUIIO buffer, Fig. 7). At 1100°C and 3 kilobars, a rock with $X_{\text{Fe}}^{\text{Opx}} = 0.50$ will coexist with ilmenite with $X_{\text{Hem}} = 0.131$ and magnetite with $X_{\text{Usp}} = 0.549$ (according to the QUILF program of Andersen *et al.* 1993). An increase in silica activity will drive the rock toward the QUIIOp surface. If the magnetite in the rock is less than 2% of the volume of the orthopyroxene in the rock, the X_{Fe} of the silicate will not be affected by the reaction (if $\text{Mgt}/\text{Opx} = 0.02$, the orthopyroxene will decrease from $X_{\text{Mg}} = 0.50$ to $X_{\text{Mg}} = 0.496$), and the reaction path will follow the black arrow in Figure 7. For larger proportions of magnetite over orthopyroxene, the final orthopyroxene will be correspondingly more Fe-enriched, but even if the magnetite: orthopyroxene volume ratio is 0.15, the resulting X_{Fe} of the orthopyroxene when magnetite is consumed will only change from 0.50 to 0.475 (gray arrow on Fig. 7). This oxidation event could deplete magnetite from the rock and cause increases in the Fe_2O_3 component of the ilmenite. For rocks with a relatively Mg-rich orthopyroxene (for Fig. 7, this would be around $X_{\text{Fe}}^{\text{Opx}} < 0.45$), the ilmenite coexisting with quartz will contain more than 20% of the Fe_2O_3 component and should exsolve hematite on cooling.

Although the details will be different depending on the temperature and starting $X_{\text{Fe}}^{\text{Opx}}$ used, this simple

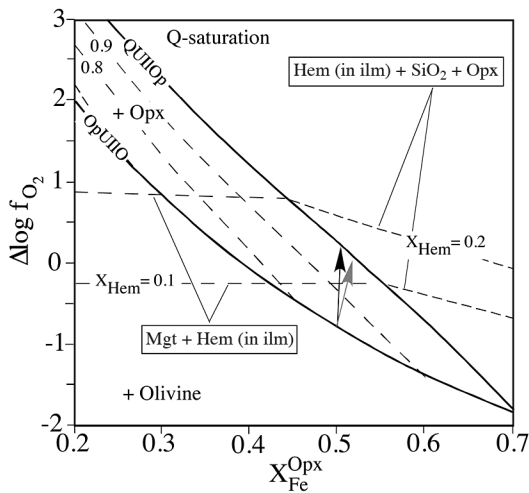


FIG. 7. $\Delta \log f(\text{O}_2)$ (relative to FMQ) versus fictive $X_{\text{Fe}}^{\text{Opx}}$ diagram showing relations among magnetite–ilmenite, pyroxene, olivine, and quartz calculated at 1000°C and 3 kilobars. QUIIOp: quartz – ulvöspinel – ilmenite – orthopyroxene. The heavy line labeled QUIIOp indicates the locus of saturation in quartz, dashed lines give the location of the QUIIOp curve at lower silica activities of 0.9, 0.8, and 0.7. Also shown are two contours for ilmenite composition showing how ilmenite becomes richer in the Fe_2O_3 component as oxygen fugacity increases. Dark arrow shows path followed during the assimilation of silica by a rock with olivine + orthopyroxene + magnetite + ilmenite in which pyroxene is far more abundant than magnetite. Gray line shows trajectory followed if the modal abundance of magnetite or pyroxene is 0.20. Calculations from the QUILF program of Anderson *et al.* (1993).

model leads us to predict four important conclusions for a system where a mafic rock reacts with a silica-rich assimilant:

1) Oxygen fugacity will increase. The extent of this increase will be dependent on X_{Fe} of the original silicate minerals. Relatively more magnesian rocks will become more intensely oxidized. This is because at all temperatures the OpUIIO and QUIIOp curves get progressively closer in $f(\text{O}_2)$ with increasing $X_{\text{Fe}}^{\text{Opx}}$. Rocks reacting at lower temperatures will be more strongly oxidized by this process because, as noted above, OpUIIO and QUIIOp slide to higher fugacities of oxygen with lower temperatures.

2) Magnetite will be consumed, and ilmenite will become more abundant.

3) Ilmenite will become enriched in Fe_2O_3 . For rocks with original X_{Fe} of orthopyroxene less than around 0.40–0.45, the ilmenite may become rich enough in the hematite component to exsolve hematite on cooling (*i.e.*, $X_{\text{Hem}} = 0.20$). The relatively low X_{Hem} in the ilmenite from Snow Creek is probably an indication that the rocks were not very close to silica saturation or that the assimilation took place at temperatures well above 1000°C.

4) Orthopyroxene will become enriched in $\text{Fe}_2\text{Si}_2\text{O}_6$, but only marginally so unless the magma initially contained very large proportions of magnetite to orthopyroxene.

The oxygen fugacity and silica activity in LAC anorthosite plutons

We can use these relations to understand the different oxygen fugacities recorded by the anorthositic plutons in the LAC (Fig. 8a). The Poe Mountain anorthosite is olivine-saturated throughout and lies upon the OpUIIO surface. Because it lies on the OpUIIO surface, the iron-enrichment trend associated with differentiation caused the Poe Mountain anorthosite to lie at progressively lower relative oxygen fugacity (Fig. 8A) and higher relative activity of silica (Fig. 8B). The Chugwater anorthosite is dominated by the assemblage Opx (or Pig)–Aug–Mgt–Ilm, and thus lies at oxygen fugacities between those of the OpUIIO and QUIIOp surfaces. Olivine only is present in the relatively magnesian troctolitic intrusions (which also contain minor orthopyroxene), and quartz is present in the most iron-rich rocks. We show the trajectory to lie as a band that runs from slightly below OpUIIO for the troctolites to QUIIOp at the most iron-rich conditions.

The Snow Creek anorthosite is dominated by the assemblage Opx (or Pig)–Aug–Ilm. Some of the samples are quartz-bearing, but the quartz does not have a magmatic texture, indicating that the original magma was near but not quite at quartz saturation. The absence of magnetite indicates that the rocks were relatively oxidized, but the low X_{Hem} in the ilmenite suggests that they were not near the QUIIOp surface.

We show the field for the Snow Creek anorthosite in dashed lines in Figure 8 because the only lower limits for oxygen fugacity that we can be certain of would be olivine saturation.

Because silica activity and oxygen fugacity are covariants, we can display the same information on a plot of silica activity versus $X_{\text{Fe}}^{\text{Opx}}$ (Fig. 8B). Because the Poe Mountain anorthosite is olivine-saturated, iron-enrichment during differentiation caused silica activity to increase. An increase in silica activity is also seen in the Chugwater anorthosite, but because it does not contain olivine, this trend was not internally controlled and probably reflects crustal contamination in the most Fe-rich portions of the anorthosite, which are the outermost portions of the intrusion. We do not see any clear trend in silica activity with respect to pyroxene composition in the Snow Creek anorthosite; as noted above, the only obvious trend is the fact that the western body is quartz-saturated, whereas the eastern one is not.

Oxygen fugacity and silica activity in Canadian anorthosites

The anorthosites of the Nain Plutonic Suite, Labrador, show similar trends to those of the LAC. The troctolitic Kiglapait intrusion contains orthopyroxene only as a rim on olivine. The Fe–Ti oxide minerals appear at a point at which olivine is Fo_{60} , which is equivalent to a fictive $X_{\text{Fe}}^{\text{Opx}} = 0.332$. On Figure 8C, we show it to lie close to but slightly below the OpUIIO surface. Many anorthositic rocks from Harp Lake, Labrador (Emslie 1980), like the Poe Mountain anorthosites, are olivine-saturated and lie on the OpUIIO surface. Magmas that crystallized both the Kiglapait intrusion and Harp Lake anorthosites underwent relative reduction (Fig. 8C) and increases in silica activity (Fig. 8D) during differentiation. The Nain anorthosite in the Puttualaak Lake area lacks olivine (Ranson 1981) and hence lies between the OpUIIO and QUIIOp curves. Ranson (1981) reported a tight cluster of pyroxene compositions for anorthosites with one outlier. For this reason, we show two fields for the Puttualaak Lake area in Figures 8C and 8D. The heavy stippling is the field where most of the pyroxene compositions fall; the light stippling extends the field to encompass the outlier. Ranson (1981) reported that some samples from the Puttualaak Lake area are quartz-saturated and that the Fe–Ti oxide assemblage is ilmenite \pm magnetite. It is possible that, like the Chugwater anorthosite, the anorthosites of the Puttualaak Lake region have assemblages that record a distinct trajectory in oxygen fugacity or silica activity, but that information cannot be derived from the information provided in Ranson (1981).

Finally, the Labrieville anorthosite is a classic example of an andesine anorthosite. It has the assemblage orthopyroxene – augite – ilmenite (Owens & Dymek 2001). Most of the samples are quartz-saturated, and small amounts of magnetite are present in the leuco-

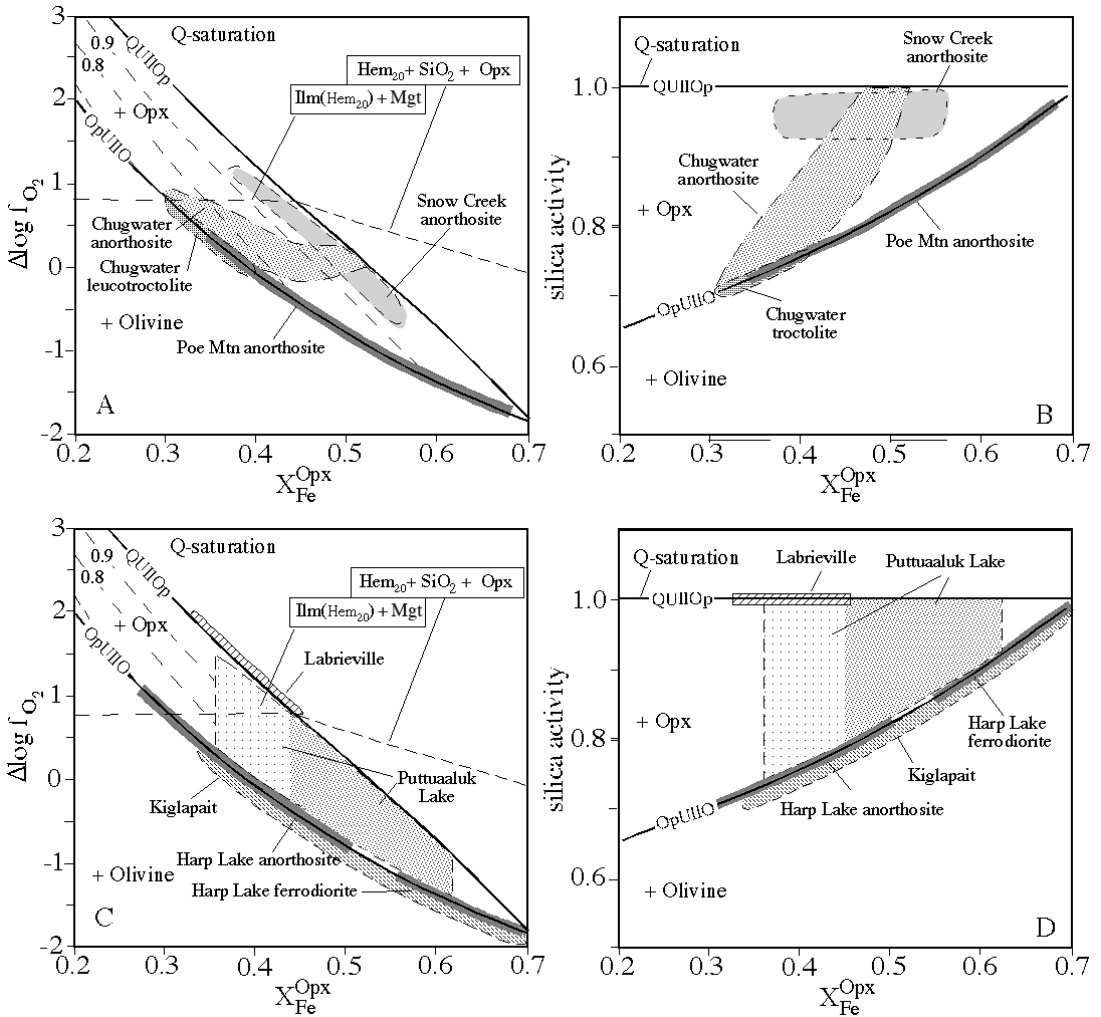


FIG. 8. A) $\Delta \log f(\text{O}_2)$ (relative to FMQ) versus fictive $X_{\text{Fe}}^{\text{Opx}}$ diagram and B) silica activity versus fictive $X_{\text{Fe}}^{\text{Opx}}$ showing the conditions of crystallization of anorthositic plutons in the Laramie Anorthosite Complex. Data from Frost & Lindsley (1992), Lindsley *et al.* (2010), and this study. C) $\Delta \log f(\text{O}_2)$ versus fictive $X_{\text{Fe}}^{\text{Opx}}$ diagram and D) silica activity versus fictive $X_{\text{Fe}}^{\text{Opx}}$ showing the crystallization conditions of the Nain plutonic suite and the Labrieville anorthosite. Data from Emslie (1980), Ranson (1981), and Owens & Dymek (2005).

gabbros. It lies on or near the QUIOP surface (Fig. 8C), but unlike the quartz-saturated rocks of Snow Creek, the Labrieville anorthosite contains exsolved ferrian ilmenite (“hemo-ilmenite”). We maintain that this is because most of the Labrieville anorthosite is considerably more magnesian than the Snow Creek, which means that increases in silica activity would have driven the Labrieville to much higher fugacity of oxygen than the more iron-rich rocks of Snow Creek [Note that contrary to the convention of Owens & Dymek (2001), the Labrieville anorthosite is not an *alkalic* anorthosite. As introduced by Peacock (1931), the term *alkalic* has a

distinct petrologic definition. As defined by the modified alkali–lime index of Frost *et al.* (2001), the Labrieville anorthosite, if anything, is alkali–calcic.]

SUMMARY AND CONCLUSIONS

In this study, we have shown that the three anorthositic plutons of the Laramie Anorthosite Complex contain assemblages that record a range of silica activities and oxygen fugacities, and that this range is likely a product of variable amounts of crustal assimilation of mantle-derived magmas. Because the parental magmas

to the LAC plutons formed in a very narrow window of space and time, we suggest that these variations in silica activity and oxygen fugacity are not primarily a function of differences in the composition of parental melts derived from the mantle-source region. Instead, we have shown how the addition of silica by crustal contamination produces both the variations in silica activity and oxygen fugacity in the LAC. The opportunities for crustal assimilation prior, during, and following differentiation of anorthositic intrusions are shown schematically on Figure 9. Because gabbroic and troctolitic magmas from the LAC did not pond and differentiate at depth, they experienced less interaction with crust than the anorthositic plutons. In contrast, the Snow Creek anorthosite, the most oxidizing and silica-rich of the anorthosite plutons, also has Nd and Sr isotopic compositions indicating incorporation of the greatest amount of a crustal component. By extension, the hypothesis that silica activity and oxygen fugacity, and the resulting mineral assemblages in cumulate anorthosites, are controlled by assimilation of continental crust also must be considered for other massif anorthosites. Isotopic identification of assimilation, especially based on the Sr and Nd isotopic systems, can be difficult where anorthosite intrudes juvenile crust that was extracted from the mantle a few tens to hundreds of millions of years prior to anorthosite magmatism (*e.g.*, in the Grenville province); however, the mineral assemblages of Proterozoic anorthosites are especially sensitive to changes in extent of crustal assimilation irrespective of the age of the underlying and enclosing crust.

The major-element chemistry of anorthosites represents a poor record of crustal assimilation, because addition of a granitic melt to a crystallizing pluton dominated by feldspar will not greatly affect the weight percent of the major oxides. For this reason, Morse (2006) could successfully invert the major-element compositions of plagioclase crystals from Nain anorthosites and identify an olivine-normative parent magma to the troctolitic rocks and a silica-saturated parent magma for the noritic suite. Experimental data allowed Morse (2006) to relate both suites to a cotectic parent magma. Isotopic results from the Nain Plutonic Suite indicate that the troctolitic rocks underwent comparatively little crustal contamination upon ascent, but the anorthositic rocks assimilated a greater volume of wallrock during their residence time in the lower crust (Emslie *et al.* 1994). In contrast, the trace-element budget of a rock dominated by plagioclase may be more strongly affected by input from a felsic assimilant. We caution that these effects must be explicitly quantified and taken into account to obtain accurate models based upon inversion of the trace-element contents of anorthosites (*e.g.*, Bédard 2001). Because of their cumulate nature and multistage petrogenesis, describing the origin and evolution of massif anorthosites and the nature of the parent magma(s) is challenging. Nevertheless, this study has shown how crustal assimilation strongly affects both silica activity and oxygen fugacity of the parent magmas to anorthositic rocks and how a range of mineral assemblages and Sr–Nd isotopic compositions can be produced from magmas that share a common mantle-derived lineage.

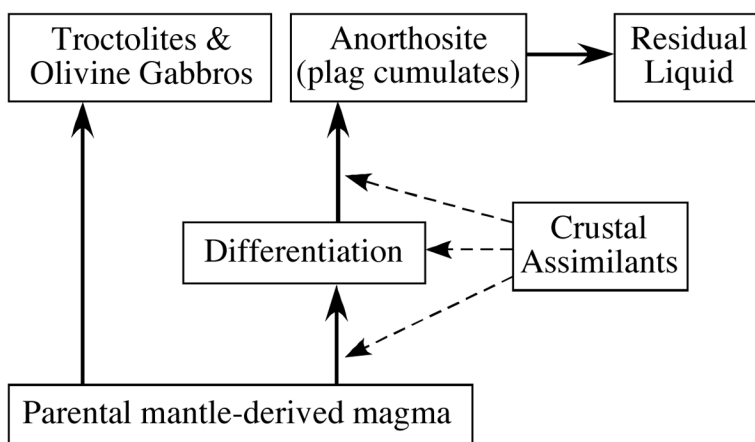


FIG. 9. Schematic diagram showing the opportunities for assimilation of crust prior, during, and following differentiation of anorthosite intrusions. Because olivine gabbros and troctolites do not pond and differentiate at depth in the crust, they may experience less interaction with crust during ascent.

ACKNOWLEDGEMENTS

This research was supported by grants EAR-9017465 and EAR-9218360 to B.R. Frost and C.D. Frost, and EAR-9218329 and its predecessors to D.H. Lindsley. We are pleased to dedicate this paper to the memory of Ron Emslie, whose comprehensive study of anorthosites and related rocks, including field, petrologic, geochemical and isotopic aspects, was the inspiration for us to do likewise.

REFERENCES

- ALLMENDINGER, R.W., BREWER, J.A., BROWN, L.D., KAUFMAN, S., OLIVER, J.E. & HOUSTON, R.S. (1982): COCORP profiling across the Rocky Mountain Front in southern Wyoming. 2. Precambrian basement structure and its influence on Laramide deformation. *Geol. Soc. Am., Bull.* **93**, 1253-1263.
- ANDERSEN, D.J., LINDSLEY, D.H. & DAVIDSON, P.M. (1993): QUILF: a Pascal program to assess equilibria among Fe-Mg-Ti oxides, pyroxenes, olivine, and quartz. *Comput. Geosci.* **19**, 1333-1350.
- ANDERSON, A.T., JR. & MORIN, M. (1969): Two types of massif anorthosites and their implications regarding the thermal history of the crust. In *Origin of Anorthosite and Related Rocks* (Y.E. Isachsen, editor). *New York State Museum and Science Service, Mem.* **18**, 57-69.
- ANDERSON, I.C., FROST, C.D. & FROST, B.R. (2003): Petrogenesis of the Red Mountain pluton, Laramie anorthosite complex, Wyoming: implications for the origin of A-type granite. *Precamb. Res.* **124**, 243-267.
- BÉDARD, J.H. (2001): Parental magmas of the Nain Plutonic Suite anorthosites and mafic cumulates: a trace element modeling approach. *Contrib. Mineral. Petrol.* **141**, 747-771.
- BLACK, L.P., KAMO, S.L., ALLEN, C.M., DAVIS, D.W., ALEINIKOFF, J.N., VALLEY, J.W., MUNDIL, R., CAMPBELL, I.H., KORSCH, R.J., WILLIAMS, I.S. & FOU DOULIS, C. (2004): Improved $^{206}\text{Pb}/^{238}\text{U}$ microprobe geochronology by the monitoring of a trace-element-related matrix effect; SHRIMP, ID-TIMS, ELA-ICP-MS and oxygen isotope documentation for a series of zircon standards. *Chem. Geol.* **205**, 115-140.
- CHAMBERLAIN, K.R. (1998): Medicine Bow orogeny: timing of deformation and model of crustal structure produced during continent-arc collision, ca. 1.78 Ga, southeastern Wyoming. *Rocky Mountain Geol.* **33**, 259-277.
- EDWARDS, B.R. & FROST, C.D. (2000): An overview of the petrology and geochemistry of the Sherman batholith, southeastern Wyoming: identifying multiple sources of Mesoproterozoic magmatism. *Rocky Mountain Geol.* **35**, 113-137.
- EMSLIE, R.F. (1980): Geology and petrology of the Harp Lake Complex, central Labrador: an example of Elsonian magmatism. *Geol. Surv. Can., Bull.* **293**.
- EMSLIE, R.F., HAMILTON, M.A. & THÉRIAULT, R.J. (1994): Petrogenesis of a mid-Proterozoic anorthosite - mangerite - charnockite - granite, AMCG complex: isotopic and chemical evidence from the Nain Plutonic Suite. *J. Geol.* **102**, 539-558.
- FROST, B.R. & LINDSLEY, D.H. (1992): Equilibria among Fe-Ti oxides, pyroxenes, olivine, and quartz. II. Application. *Am. Mineral.* **77**, 1004-1020.
- FROST, C.D., BELL, J.M., FROST, B.R. & CHAMBERLAIN, K.R. (2001): Crustal growth by magmatic underplating: isotopic evidence from the northern Sherman batholith. *Geology* **29**, 515-518.
- FROST, C.D., CHAMBERLAIN, K.R., FROST, B.R. & SCOATES, J.S. (2000): The 1.76-Ga Horse Creek anorthosite complex, Wyoming: a massif anorthosite emplaced late in the Medicine Bow orogeny. *Rocky Mountain Geol.* **35**, 71-90.
- FROST, C.D., FROST, B.R., BELL, J.M. & CHAMBERLAIN, K.R. (2002): The relationship between A-type granites and residual magmas from anorthosite: evidence from the northern Sherman batholith, Laramie Mountains, Wyoming, USA. *Precamb. Res.* **119**, 45-71.
- FROST, C.D., FROST, B.R., CHAMBERLAIN, K.R. & EDWARDS, B.R. (1999): Petrogenesis of the 1.43 Ga Sherman batholith, SE Wyoming, USA: a reduced, rapakivi-type anorogenic granite. *J. Petrol.* **40**, 1771-1802.
- FUHRMAN, M.L., FROST, B.R. & LINDSLEY, D.H. (1988): Crystallization conditions of the Sybille monzosyenite, Laramie Anorthosite Complex, Wyoming. *J. Petrol.* **29**, 699-729.
- GEIST, D.J., FROST, C.D. & KOLKER, A. (1990): Sr and Nd isotopic constraints on the origin of the Laramie anorthosite complex, Wyoming. *Am. Mineral.* **75**, 13-20.
- GEIST, D.J., FROST, C.D., KOLKER, A. & FROST, B.R. (1989): A geochemical study of magmatism across a major terrane boundary: Sr and Nd isotopes in Proterozoic granitoids of the southern Laramie Range, Wyoming. *J. Geol.* **97**, 331-342.
- GOLDBERG, S.A. (1984): Geochemical relationships between anorthosite and associated iron-rich rocks, Laramie Range, Wyoming. *Contrib. Mineral. Petrol.* **87**, 376-387.
- HÉBERT, C., CADIEUX, A.-M. & VAN BREEMEN, O. (2005): Temporal evolution and nature of Ti-Fe-P mineralization in the anorthosite - mangerite - charnockite - granite (AMCG) suites of the south-central Grenville Province, Saguenay - Lac St. Jean area, Quebec, Canada. *Can. J. Earth Sci.* **42**, 1865-1885.
- HIGGINS, M.D. & VAN BREEMEN, O. (1992): The age of the Lac-Saint-Jean anorthosite complex and associated mafic rocks, Grenville Province, Canada. *Can. J. Earth Sci.* **29**, 1412-1423.

- KOLKER, A., FROST, C.D., HANSON, G.N. & GEIST, D.J. (1991): Neodymium, strontium, and lead isotopes in the Maloin Ranch pluton, Wyoming: implications for the origin of evolved rocks at anorthosite margins. *Geochim. Cosmochim. Acta* **55**, 2285-2297.
- KOLKER, A. & LINDSLEY, D.H. (1989): Geochemical evolution of the Maloin Ranch pluton, Laramie anorthosite complex, Wyoming: petrology and mixing relations. *Am. Mineral.* **74**, 307-324.
- KOLKER, A., LINDSLEY, D.H. & HANSON, G.N. (1990): Geochemical evolution of the Maloin Ranch pluton, Laramie anorthosite complex, Wyoming: trace elements and petrogenetic models. *Am. Mineral.* **75**, 572-588.
- KROGH, T.E. (1973): A low-contamination method for hydrothermal decomposition of zircon and extraction of U and Pb for isotopic age determinations. *Geochim. Cosmochim. Acta* **37**, 485-494.
- LAFRANCE, B., JOHN, B.E. & FROST, B.R. (1998): Ultra high-temperature shear zones: examples from the Poe Mountain anorthosite, Wyoming. *J. Struct. Geol.* **20**, 945-955.
- LINDSLEY, D.H. & FROST, B.R. (1992): Equilibria among Fe-Ti oxides, pyroxenes, olivine and quartz. I. Theory. *Am. Mineral.* **77**, 987-1003.
- LINDSLEY, D.H., FROST, B.R., FROST, C.D. & SCOATES, J.S. (2010): Petrology, geochemistry, and structure of the Chugwater anorthosite, Laramie anorthosite complex, southeastern Wyoming. *Can. Mineral.* **48**, 887-923.
- LUDWIG, K.R. (1988): PbDAT for MSDOS: a computer program for IBM-PC compatibles for processing raw Pb-U-Th isotope data, version 1.24. *U.S. Geol. Surv., Open-File Rep.* **88-542**.
- LUDWIG, K.R. (1991): ISOPLOT for MSDOS: a plotting and regression program for radiogenic isotope data for IBM-PC compatible computers, version 2.75. *U.S. Geol. Surv., Open-File Rep.* **91-445**.
- MITCHELL, J.N. (1993): *Petrology and Geochemistry of Dioritic and Gabbroic Rocks in the Laramie Anorthosite Complex, Wyoming: Implications for the Evolution of Proterozoic Anorthosite*. Ph.D. thesis, University of Wyoming, Laramie, Wyoming, USA.
- MITCHELL, J.N., SCOATES, J.S. & FROST, C.D. (1995): High-Al gabbros in the Laramie anorthosite complex, Wyoming: implications for the composition of melts parental to Proterozoic anorthosite. *Contrib. Mineral. Petrol.* **119**, 166-180.
- MITCHELL, J.N., SCOATES, J.S., FROST, C.D. & KOLKER, A. (1996): The geochemical evolution of anorthosite residual magmas in the Laramie anorthosite complex, Wyoming. *J. Petrol.* **37**, 637-660.
- MORSE, S.A. (2006): Labrador massif anorthosites: chasing the liquids and their sources. *Lithos* **89**, 202-221.
- OWENS, B.E. & DYMEK, R.F. (2001): Petrogenesis of the Labrieville alkalic anorthosite massif, Grenville Province, Quebec. *J. Petrol.* **42**, 1519-1546.
- OWENS, B.E. & DYMEK, R.F. (2005): Rediscovery of the Mattawa anorthosite massif, Grenville Province, Quebec. *Can. J. Earth Sci.* **42**, 1699-1718.
- OWENS, B.E., DYMEK, R.F., TUCKER, R.D., BRANNON, J.C. & PODOSEK, F.A. (1994): Age and radiogenic isotopic composition of a late- to post-tectonic anorthosite in the Grenville Province: the Labrieville massif, Quebec. *Lithos* **31**, 189-206.
- PARRISH, R.R., RODDICK, J.C., LOVERIDGE, W.D. & SULLIVAN, R.D. (1987): Uranium-lead analytical techniques at the geochronology laboratory, Geological Survey of Canada. In *Radiogenic Age and Isotopic Studies, Report 1. Geol. Surv. Can., Pap.* **87-2**, 3-7.
- PEACOCK, M.A. (1931): Classification of igneous rock series. *J. Geol.* **39**, 54-67.
- RANSON, W.A. (1981): Anorthosites of diverse magma types in the Puttualaak Lake area, Nain Complex, Labrador. *Can. J. Earth Sci.* **18**, 26-41.
- SCOATES, J.S. (1994): *Magmatic Evolution of Anorthositic and Monzonitic Rocks in the Mid-Proterozoic Laramie Anorthosite Complex, Wyoming, USA*. Ph.D. thesis, University of Wyoming, Laramie, Wyoming, USA.
- SCOATES, J.S. (2000): The plagioclase - magma density paradox re-examined and the crystallization of Proterozoic anorthosites. *J. Petrol.* **41**, 627-649.
- SCOATES, J.S. & CHAMBERLAIN, K.R. (1995): Baddeleyite (ZrO₂) and zircon (ZrSiO₄) from anorthositic rocks of the Laramie anorthosite complex, Wyoming: petrologic consequences and U-Pb ages. *Am. Mineral.* **80**, 1317-1327.
- SCOATES, J.S. & CHAMBERLAIN, K.R. (1997): Orogenic to post-orogenic origin for the 1.76 Ga Horse Creek anorthosite complex, Wyoming, USA. *J. Geol.* **105**, 331-343.
- SCOATES, J.S. & CHAMBERLAIN, K.R. (2003): Geochronologic, geochemical and isotopic constraints on the origin of monzonitic and related rocks in the Laramie anorthosite complex, Wyoming, USA. *Precamb. Res.* **124**, 269-304.
- SCOATES, J.S. & FROST, C.D. (1996): A strontium and neodymium isotopic investigation of the Laramie anorthosites, Wyoming, USA: implications for magma chamber processes and the evolution of magma conduits in Proterozoic anorthosites. *Geochim. Cosmochim. Acta* **60**, 95-107.
- SCOATES, J.S., FROST, C.D., MITCHELL, J.N., LINDSLEY, D.H. & FROST, B.R. (1996): Residual-liquid origin for a monzonitic intrusion in a mid-Proterozoic anorthosite complex: the Sybille intrusion, Laramie anorthosite complex, Wyoming. *Geol. Soc. Am., Bull.* **108**, 1357-1371.
- SCOATES, J.S., LINDSLEY, D.H. & FROST, B.R. (2010): Magmatic and structural evolution of an anorthositic magma

- chamber: the Poe Mountain intrusion, Laramie Anorthosite Complex, Wyoming (USA). *Can. Mineral.* **48**, 851-885.
- STACEY, J.S. & KRAMERS, J.D. (1975): Approximation of terrestrial lead isotope evolution by a two-stage model. *Earth Planet. Sci. Lett.* **26**, 207-221.
- STEIGER, R.H. & JÄGER, E. (1977): Subcommittee on geochronology: convention on the use of decay constants in geo- and cosmochronology. *Earth Planet. Sci. Lett.* **36**, 359-362.
- SUBBARAYUDU, G.V., HILLS, F.A. & ZARTMAN, R.E. (1975): Age and Sr isotopic evidence for the origin of the Laramie anorthosite-syenite complex, Laramie Range, Wyoming. *Geol. Soc. Am., Abstr. Programs* **7**, 1287.
- VERTS, L.A., CHAMBERLAIN, K.R. & FROST, C.D. (1996): U-Pb sphene dating of metamorphism: the importance of sphene growth in the contact aureole of the Red Mountain pluton, Laramie Mountains, Wyoming. *Contrib. Mineral. Petrol.* **125**, 186-199.
- WAKITA, H., REY, P. & SCHMITT, R.A. (1971): Abundances of the 14 rare-earth elements and 12 other trace elements in Apollo 12 samples: five igneous and one breccia rocks and four soils. *In Proc. Second Lunar Science Conf.* **2** (A.A. Levinson, ed.). MIT Press, Cambridge, Massachusetts (1319-1329).
- XUE, SUZHOU & MORSE, S.A. (1993): Geochemistry of the Nain massif anorthosite, Labrador: magma diversity in five intrusions. *Geochim. Cosmochim. Acta* **57**, 3925-3948.

Received December 18, 2008, revised manuscript accepted July 4, 2010.